The AKAP220 signaling complex regulates renal aquaporin-2 localization

Jennifer L Whiting

A dissertation
submitted in partial fulfillment of the
requirements for the degree of

Doctor of Philosophy

University of Washington
2015

Reading Committee:
John D. Scott (Chair)
Richard Gardner
Linda Wordeman

Program Authorized to Offer Degree:
Pharmacology

University of Washington

Abstract

The AKAP220 signaling complex regulates renal aquaporin-2 localization

Jennifer Lee Whiting

Chair of the Supervisory Committee:
Professor John D. Scott
Department of Pharmacology

A kinase anchoring proteins (AKAPs) localize signaling molecules such as kinases and phosphatases in close proximity to their substrates to control the scope and duration of second messenger responses. AKAP220 is a ubiquitously expressed, 220-kilodalton protein that anchors protein kinase A (PKA), glycogen synthase kinase 3β (GSK3β) and protein phosphatase 1 (PP1). Although AKAP220 has been implicated in promoting cortical actin polymerization, little is currently known about the biological function of this signaling complex.

To gain insight toward this question, we used biochemical and cell based assays to explore the kinase anchoring dynamics of AKAP220. We discovered that AKAP220 preferentially anchors catalytically active GSK3β within a 17-amino acid linear region containing a required GSK3β phosphosite. We also identified a novel PKA anchoring helix in the amino terminus of AKAP220 and characterize the isoform-binding properties of both PKA sites. Within the complex, activation of anchored PKA inhibits GSK3β activity and opposes its binding to AKAP220.

Using Cre-lox technology, we produced a global AKAP220 knockout mouse model to study the functional role of AKAP220 *in vivo*. We find that loss of AKAP220 causes a urine-diluting deficit in response to acute water loading. Based on immunostaining experiments, we propose that this phenotype is caused by the abnormal accumulation of aquaporin-2 (AQP2) at the apical plasma membrane of renal principal cells. This mislocalization is consistent with our pulldown assays detecting a decrease in GTP-bound (active) RhoA in AKAP220 knockout kidneys.

RhoA activity promotes the formation of an apical actin barrier in renal principal cells. This actin meshwork prevents basal fusion of AQP2-containing vesicles in the absence of vasopressin stimulation. Previous studies have shown that AKAP220 promotes polymerization of cortical actin, so we investigated whether this complex may influence actin barrier formation in the kidney. Using CRISPR-Cas9 genome editing technology we generated mIMCD3 cells that do not express AKAP220. These cells were grown in 3D culture to produce polarized spheroids. Imaging analysis of these spheroids revealed that AKAP220$^{-/-}$ cells had decreased apical actin thickness compared to wild-type. Together, these findings indicate that AKAP220 anchors signaling elements that influence AQP2 localization in the collecting duct of mammalian kidneys.

Table of Contents

List of Figures

List of Tables:

Glossary

Name	Abbreviation
AKAP	A kinase anchoring protein
8-bromo cAMP	8-Bromoadenosine 3',5'-cyclic monophosphate
Akt	protein kinase B
AQP2	aquaporin-2
AVP	arginine vasopressin
cAMP	cyclic adenosine monophosphate
Cdc42	Cell division control protein 42 homolog
CDI	central diabetes insipidus
EDTA	ethylene diamine tetraacetic acid
EGTA	ethylene glycol tetraacetic acid
ES cell	embyonic stem cell
FACS	fluorescence activated cell sorting
FITC	fluorescein isothiocyanate
FP	fluorescence polarization
g	grams
G418	Geneticin
GSK3β	glycogen synthase kinase 3β
HRP	horse radish peroxidase
IMCD	inner medullary collecting duct
IQGAP	IQ domain containing GTPase activating protein
Kd	dissociation constant
MALS	multi angle light scattering
mIMCD3	mouse inner medullary collecting duct cell line
mP	millipolarization unit
NDI	nephrogenic diabetes insipidus
NaCl	sodium chloride
Neo	neomycin
PBS	phosphate buffered saline
PCR	polymerase chain reaction
PDGF	platelet derived growth factor

PFA	paraformaldehyde
PKA	protein kinase A
PLA	proximity ligation assay
PP1	protein phosphatase 1
Rac1	Ras-related C3 botulinum toxin substrate 1
RI	PKA regulatory subunit type I
RII	PKA regulatory subunit type II
ROI	region of interest
SCC	saline sodium citrate
SDS	sodium dodecyl sulfate
Ser	serine
SiMPull	single molecule pulldown
SKIP	sphingosine kinase interacting protein
Thr	threonine
V2R	vasopressin type 2 receptor
µm	micrometer
µM	micromolar

Acknowledgements

I would like to thank John Scott for giving me the opportunity to conduct this work and providing me with mentorship and guidance throughout my graduate career. I would also like to thank my thesis committee Rich Gardner, Linda Wordeman, Sandy Bajjalieh, and Larry Zweifel. My project has changed a great deal over the years, yet you have continually supported and encouraged my journey.

I also want to thank the UW Department of Comparative Medicine, especially Serina Tsang and Bob Hunter. Your expertise with embryonic stem cells and knockout mouse production was invaluable to my work.

To the members of the Scott lab, both past and present, thank you for everything you have taught me and for answering my endless questions. A special thank you to my fellow graduate students, Patrick Nygren and Bret Samelson. Thanks for the afternoon cookie breaks, the endless laughs, and the support you gave me over the years. Also, thanks to my classmates and fellow students. I consider myself lucky to be part of such a close-knit department, and I'm happy to have shared so memories with all of you.

To Jim Varner, thank you for all of your support. You have shared my excitement when experiments were working, and providing comfort when they (usually) weren't. Thank you for sitting through so many practice talks that you could probably recite them from memory. Your enthusiasm for my work has given me confidence, and I can't thank you enough for that.

Finally, I want to thank my parents and biggest cheerleaders, Chris and Deb Whiting. I could never have come this far without your love and endless support. You have always believed in me, even when I have doubted myself. Words can't express my gratitude for all the opportunities that you have given me. You are the inspiration for my success, and I am so thankful for everything you have done to help me achieve my dreams.

Preface

Portions of the text and data from this dissertation are reproduced from the following previously published work under fair use:

Whiting JL, Nygren PJ, Tunquist BJ, Langeberg LK, Seternes OM, Scott JD. Protein Kinase A Opposes the Phosphorylation-Dependent Recruitment of Glycogen Synthase Kinase 3β to A-Kinase Anchoring Protein 220. *J. Biol. Chem.* 2015 (*in press*). © the American Society for Biochemistry and Molecular Biology.

Chapter 1

Introduction to AKAP220

Cellular communication is a biological requirement for all life forms. Any cellular process that converts a stimulus into a response is referred to as signal transduction. These events typically occur through rapid biochemical reactions involving a combination of second messenger molecules and protein catalysts called enzymes[1]. Single-celled organisms use these signaling pathways to sense their environment and adapt to the chemical cues in their surroundings. As more complex multicellular organisms have evolved, the complexity of the signal transduction pathways has increased accordingly. Interestingly, many of the major signaling enzymes are conserved throughout evolution, from bacteria to humans[2]. Because some signal transduction events can occur on the millisecond scale, the need for efficient and precise localization of enzymes has been accommodated by the evolution of anchoring proteins, scaffolds, and enzyme-targeting subunits [3-5].

A-kinase anchoring proteins (AKAPs) are an illustrative example of this concept. This family of proteins is defined by their ability to anchor the regulatory (R) subunits of protein kinase A (PKA) [6,7]. Most AKAPs also anchor additional signaling enzymes such as kinases, phosphatases and phosphodiesterases[8-10]. Although most AKAPs are unrelated in sequence, binding partners, and expression patterns, a universal feature of this family is to anchor signaling enzymes in close proximity to substrates. Tethering signaling pathways to discrete locations within the cell limits the scope of second

messenger signaling and allows for rapid, efficient, and often reversible modification of downstream targets[11-13].

The physiological significance of this mechanism has been validated in several cellular and *in vivo* contexts. The tetrameric PKA holoenzyme is composed of two regulatory (R) subunits and two catalytic (C) subunits[14-16]. High-resolution structural studies have revealed that the type I (RI) or type II (RII) subunits homodimerize and create a binding groove within a four-helix bundle [7,17]. An amphipathic helix within the AKAP binds to this groove with high affinity[18,19]. Electron microscopy of intact type II PKA–AKAP18γ complexes has shown that intrinsically disordered regions within each PKA regulatory subunit impart flexibility within the holoenzyme complex[20]. Therefore, it is likely that these macromolecular AKAP assemblies can adopt a range of conformations that may help to more efficiently position the PKA catalytic subunits in proximity to target substrates[20]. By anchoring PKA at defined subcellular locations, AKAPs manage the phosphorylation dependent modulation of downstream targets[21].

AKAP220 was originally discovered as an AKAP by RIIα overlay experiments with a rat pituitary cDNA library[22]. This 220-kilodalton protein is ubiquitously expressed in many cell and tissue types, and is evolutionarily conserved in mammals. Known enzymatic binding partners include PKA, glycogen synthase kinase 3β (GSK3β), and protein phosphatase 1 (PP1)[22-24]. In addition, AKAP220 has been shown to bind IQ motif containing GTPase-activating proteins (IQGAPs) and the renal water channel aquaporin-2 (AQP2)[25-27]. The known binding sites for each binding partner are listed in Table 1.1, including the newly discovered sites and characteristics described in this thesis.

Local anchoring of kinases and phosphatases promotes efficient and bi-directional control of signal transduction events. In the context of AKAP220, both PKA and GSK3β can phosphorylate nearby substrates, some of which may be also dephosphorylated by anchored PP1 in the complex. This balance of enzymatic activity can be shifted in response to second messengers such as cAMP. For example, GSK3β is active under resting conditions but is phosphorylated and inhibited by PKA in response to elevations

in cAMP[28]. Therefore, cAMP simultaneously promotes PKA signaling pathways while inhibiting GSK3β signaling pathways.

In addition to cAMP, we've also shown that calcium signaling influences AKAP220 complexes. IQGAPs bind to AKAP220 in a calcium-dependent manner, likely promoted by dissociation of calmodulin (CaM) from the IQ-domain[29]. In COS cells, ionophore A23187 treatment raises intracellular calcium and increases AKAP220 and IQGAP binding, while preparing cell lysates in the presence of calcium chelators EDTA/EGTA abolishes the interaction [26]. Calcium is a common second messenger, and it is interesting that signaling with growth hormones such as PDGF causes activation of cAMP concomitantly with calcium influx. In the context of AKAP220, this could allow for simultaneous activation of PKA and recruitment of IQGAP to the scaffold.

Unfortunately, little is currently known about the biological significance of AKAP220. Several experiments have implicated these signaling complexes in regulating cytoskeletal dynamics, and it has been linked to both the actin and microtubule networks through IQGAPs. For example, AKAP220 has been detected at the cell cortex by immunostaining in several cell types (COS, HT-1080, HEK), where it co-localizes with IQGAPs and the cortical actin cytoskeleton. IQGAP proteins have a well-established role in recruiting the small GTPases Rac1 and Cdc42 to promote lamellipodial and filopodial protrusion at the cortex [30]. Interestingly, siRNA silencing of AKAP220 reduces cortical f-actin staining and significantly diminishes membrane ruffling [25]. Subsequent experiments revealed a PKA phosphosite on IQGAP2 at Thr716 that increased recruitment of active, GTP-bound Rac1 to the signaling complex when phosphorylated. Mutational analysis demonstrated that cells expression IQGAP2-T716A had reduced membrane ruffling, while the phospho-mimetic IQGAP2-T716D form increased membrane ruffling [25].

In addition to modulating cortical actin polymerization, AKAP220 signaling also influences microtubule dynamics through IQGAP1. AKAP220-IQGAP1 complexes are localized to the leading edge of motile cells, where they promote microtubule stabilization in response to growth factor signaling. Interestingly, siRNA-mediated knockdown of AKAP220 caused mislocalization of IQGAP1 away from the cell cortex

and resulted in blunted cell migration rates and disorganized cortical microtubules. This effect was linked to mislocalization of CLIP-associating protein (CLASP2), a microtubule plus-end binding protein that also interacts with IQGAP1 at the leading edge of migrating cells. Interestingly, phosphorylation of CLASP2 by GSK3β prevents it from associating with IQGAP1 and microtubules[31]. Therefore, local inhibition of GSK3β signaling is believed to promote CLASP2-IQGAP1 binding, thereby stabilizing microtubules and supporting membrane protrusion. Consistent with this hypothesis, treating cells with the small molecule GSK3β inhibitor SB416286 increases CLASP2 localization at the tips of leading edge microtubules and enhances the formation of AKAP220-IQGAP1-CLASP2 immunocomplexes [26]. Because GSK3β and AKAP220 are both ubiquitously expressed, it is likely that these signaling complexes have multiple roles depending on the cell or tissue, developmental stage, or activated signaling pathway. For example, the studies described here have discovered an interaction between AKAP220 and β-catenin, a well-known GSK3β substrate.

Although there are known roles for the kinases associated with AKAP220, the function of anchored PP1 in this complex remains unknown. AKAP220 associates with the PP1 catalytic subunit through prototypical KVQF targeting motif [24]. In addition, a secondary binding site was discovered between AKAP220 residues 1711-1901 that was shown to inhibit PP1 activity [32]. PP1 truncation mutants were used to determine the inhibitory mechanism is distinct from other known PP1 inhibitors or toxins. Interestingly, when PKA regulatory subunit was added to the complex PP1 activity was further inhibited, suggesting the dynamic assembly of AKAP220 signaling complexes may influence the catalytic activity of its binding partners [32].

In the kidney collecting ducts, AKAP220 was found to bind the carboxy-terminal tail of the AQP2 water channel [27]. This is particularly interesting, because AKAP220 anchors several enzymes known to regulate AQP2 signaling, including PKA, GSK3β, and PP1 [33-35]. A detailed description of how these enzymes modulate AQP2 function, regulation, and trafficking can be found in the Introduction section of Chapter 4.

Although AKAP220 has been shown to interact with all of these proteins, we still have no information regarding the occupancy or stoichiometry of these complexes. It is likely

that multiple variations may form *in vivo* because AKAP220 is ubiquitously expressed in many different types of cells and tissues. For example, the region of AKAP220 that interacts with AQP2 may bind to a different protein partner in cells that do not express AQP2, and *vice versa*. For this reason, we were interested in exploring the basics of AKAP220 complex formation, with a primary focus on mapping the precise kinase binding characteristics of AKAP220.

In addition, we produced an AKAP220 conditional knockout model as a powerful tool to study the biological significance of the anchoring protein (Chapter 3). Using recombineering technology and a Cre-lox strategy, we successfully engineered mouse embryonic stem cells containing a floxed *Akap11* allele. These cells were used to generate a line of AKAP220$^{lox/lox}$ mice that are now available for breeding to any desired Cre line for production of conditional AKAP220 knockout mice. In the initial experiments described here, we utilized the EIIa-Cre line to produce a global AKAP220 knockout. We then characterized the phenotypic effects on AQP2 localization (Chapter 4).

Table 1.1 – Known AKAP220 binding partners

Protein	Known Binding Sites (amino acid position)	Additional Information	References
Protein Kinase A	Site 1: 610-623 Site 2: 1633-1646	Negatively regulates GSK3β binding	Lester, 1996 Whiting, 2015
Glycogen Synthase Kinase 3β	1126-1142	Requires phospho-Thr1132	Tanji, 2002
Protein Phosphatase 1	1187-1190 (KVQF) 2˚ contact: 1711-1901	2˚ contact site inhibits PP1 activity	Schillace, 2000 Schillace, 2001
IQGAP1 **IQGAP2**	1-508	Calcium dependent	Logue, 2011 Logue, 2011
Aquaporin-2	1085-1174	Binding site overlaps with GSK3β and PP1	Okutsu, 2008

Chapter 2

Kinase anchoring properties of AKAP220

Introduction

AKAP220 regulates cytoskeletal dynamics through an interaction with IQ motif containing GTPase activating proteins (IQGAPs) [25]. Signaling through anchored PKA and GSK3β regulates both actin polymerization and microtubule organization at the cell cortex [26]. Gene silencing of AKAP220 decreases membrane ruffling, alters microtubule organization, and slows cell migration [26]. Although AKAP220-associated PKA and GSK3β have been implicated in these cellular events, it is imperative that we obtain a more mechanistic understanding of the interplay between the enzymes in this complex.

Localized anchoring of GSK3 with basophilic kinases such as PKA is functionally relevant, as phosphorylation of serine 21 on GSK3α or serine 9 on GSK3β attenuates its catalytic activity [36]. In this study, we discover that active GSK3β phosphorylates AKAP220 to create and maintain its binding site, and that AKAP220 localizes GSK3β with its substrate β-catenin in membrane ruffles. We also identify and characterize two separate PKA binding sites on AKAP220, and show that associated PKA regulates recruitment of GSK3β in a multi-step and phosphorylation-dependent manner. This work enhances our understanding of the kinase anchoring properties of AKAP220, and highlights the importance of enzymatic crosstalk within this macromolecular signaling complex.

Results

Mapping the GSK3β binding site

GSK3β was previously discovered as an AKAP220 binding partner by yeast two-hybrid screen, and the binding interface loosely mapped to residues 1009-1305 of AKAP220[23]. Cell-based validation of this interaction was demonstrated by co-IP of endogenous GSK3β with AKAP220 from HEK293 cell lysates (Fig. 2.1A). The presence of GSK3β and the C subunit of PKA were detected by immunoblot. These data confirm that AKAP220 has the capacity to anchor PKA and GSK3β.

Next, detailed mapping of the previously identified GSK3β binding site on AKAP220 was conducted by peptide array analyses (Fig. 2.1B-C). A library of overlapping 20mer peptides (displaced by 3 amino acids) spanning residues 1009-1305 of AKAP220 was spotted onto a peptide array membrane and screened for direct interaction with purified GSK3β by far western overlay. Two GSK3β-binding peptides were detected, suggesting the interaction occurs within a minimum region encompassed by residues 1126-1142 (Fig. 2.1C). Control arrays covering the same region on AKAP220 gave negative results when probed with a catalytically inactive mutant, GSK3β-K85A [36].

A distinguishing feature of this sequence is a prevalence of proline, serine and threonine residues. Scansite analysis of AKAP220 residues 1126-1142 predicted two consensus phosphorylation sites for GSK3 (Thr1128 and Thr1132) [37]. To test whether purified GSK3β could phosphorylate one or both of these sites, overlapping AKAP220 peptides were generated by spot array and incubated with γ[^{32}P]-ATP and increasing amounts of purified kinase (from 7.5-75 ng/ul; Fig. 2.1D). Radiolabeled phosphate incorporation into the immobilized peptides was assessed by autoradiography. Peptides 1 and 2 were phosphorylated in a dose-dependent manner, but peptide 3 lacking the upstream proline-rich segment was not. Control experiments performed with a kinase-dead mutant (GSK3β-K85A) showed no phosphorylation of any of the peptides.

To determine which site was phosphorylated, an additional array of AKAP220 peptides was generated in which alanine was substituted for candidate serine and threonine residues between 1128 and 1132 of AKAP220 (Fig. 2.1E). Phosphorylation was

reduced in all peptides in which Thr1132 was replaced with alanine (Fig. 2.1E). In contrast, single substitutions at Thr1128 or Ser1131 did not affect phosphorylation by GSK3β (Fig. 2.1E). Control experiments with the GSK3β-K85A mutant confirmed that this catalytically inactive form of the enzyme was unable to phosphorylate the AKAP220 peptides. Taken together these results suggest that Thr1132 is a GSK3β phosphosite on AKAP220.

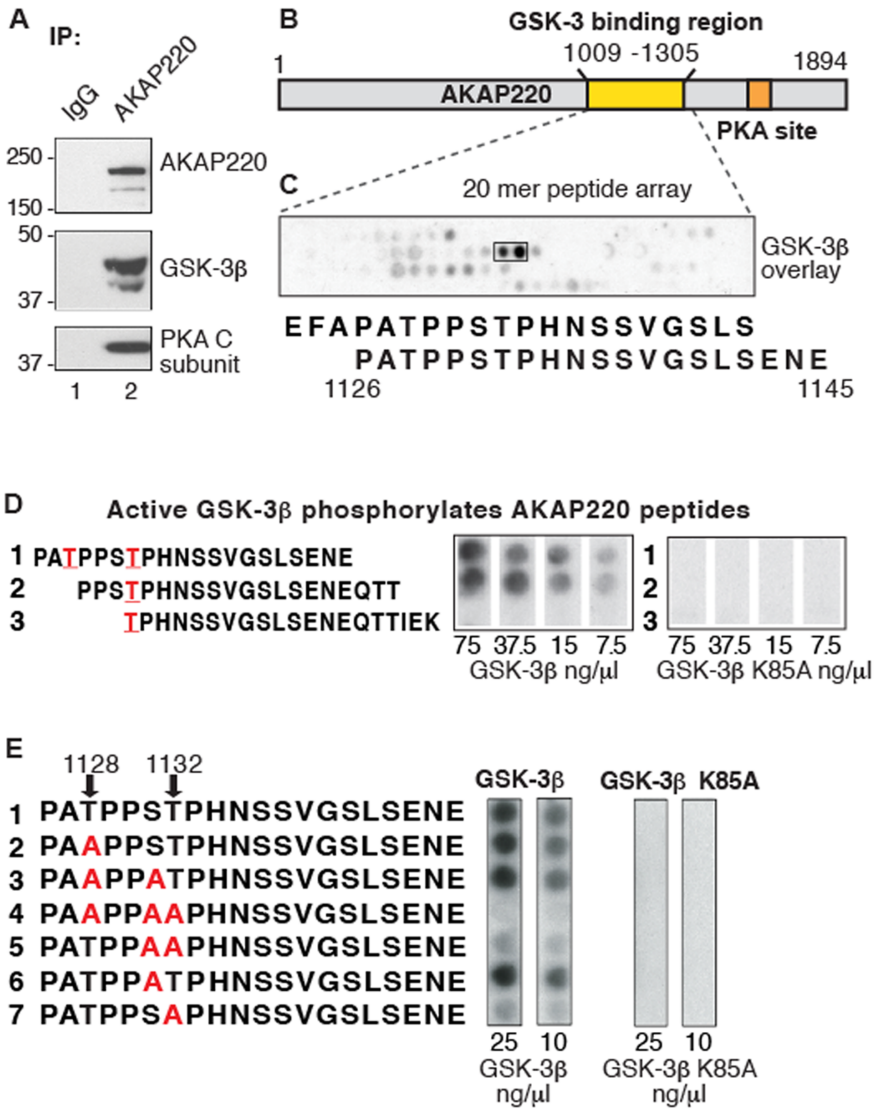

Figure 2.1 – Mapping the GSK3β binding site. A) GSK3β and PKA are both detected in AKAP220 immune complexes. B) Schematic representation of the AKAP220 protein. The GSK3 binding site was previously mapped to residues 1109-1305 (yellow). C) Overlapping 20mer peptides corresponding to this region of AKAP220 were synthesized onto cellulose by peptide array for far-western analysis. The membrane was incubated with purified GSK3β and binding detected by an anti-GSK3β antibody. Two peptides corresponding to AKAP220 residues 1123-1145 were strongly detected. D) The peptide sequence for residues 1126-1145 was again synthesized by peptide array for an *in vitro* kinase assay with purified GSK3β. Predicted GSK3β phosphosites are indicated in red. Phosphorylation was detected for peptides 1 and 2, but not peptide 3. E) Alanine mutations were introduced into this peptide sequence at Thr1128, Ser1131, and Thr1132 to map and confirm GSK3β phosphosites. Phosphorylation was unchanged when alanine was substituted for Thr1128 (peptide 2), Ser1131 (peptide 6), or both (peptide 3). However, phosphorylation was reduced in all peptides containing an alanine substitution for Thr1132.

Kinase activity drives GSK3β interaction with AKAP220

Cellular validation of GSK3β binding was confirmed by transfecting a GFP-tagged fragment of the anchoring protein (residues 1009-1305) into HEK cells. Lysates from cells expressing wild-type, T1128A, T1132A, or T1128-T1132A AKAP220 fragments were prepared and signaling complexes were isolated by immunoprecipitation with anti-GFP antibody and were probed for co-precipitation of endogenous GSK3β by immunoblot (Fig. 2.2A). These experiments revealed that mutating Thr1132 to alanine abolished GSK3β binding. However mutating Thr1128 to alanine did not effect the GSK3β interaction when compared to wild-type. Thus, Thr1132 is required for AKAP220-GSKβ interaction inside cells.

We next investigated GSK3β binding in the context of full-length AKAP220. HEK293 cells were co-transfected with plasmids encoding V5-tagged AKAP220 and either wild-type GSK3β, a kinase-dead mutant (K85A), a constitutively active mutant (S9A), or a phosphate-binding site mutant (R96A) [36]. The GSK3β-R96A mutation specifically prevents GSK3β from phosphorylating primed substrates, but has no effect on non-primed substrates such as β-catenin and Axin [28]. Immunoblot analysis revealed that AKAP220 had increased binding with the constitutively active GSK3β-S9A mutant compared to wild-type GSK3β (Fig. 2.2B). However, neither the catalytically inactive GSK3β-K85A nor the phosphate-binding site mutant GSK3β-R96A co-fractionated with AKAP220 (Fig. 2.2B). In addition, the AKAP220-T1132A mutant did not interact with wild-type or any of the mutant GSK3β forms (Fig. 2.2B). Together these data indicate the catalytic activity of GSK3β is required for binding, and that Thr1132 on AKAP220 is a GSK3β substrate required for the interaction.

In light of these results we propose a mechanism of interaction between GSK3β and AKAP220 (Fig. 2.2C). The active kinase phosphorylates AKAP220-Thr1132 to initiate complex formation. Mutating this residue to alanine abolishes GSK3β binding, indicating that Thr1132 is required and that AKAP220 interacts with a single molecule of GSK3β. Catalytic activity is also required to form the AKAP220-GSK3β complex, as the kinase-dead mutant did not associate with full length AKAP220 in cells. Additional validation of

this hypothesis comes from our evidence of enhanced AKAP220 binding to the constitutively active GSK3β-S9A mutant.

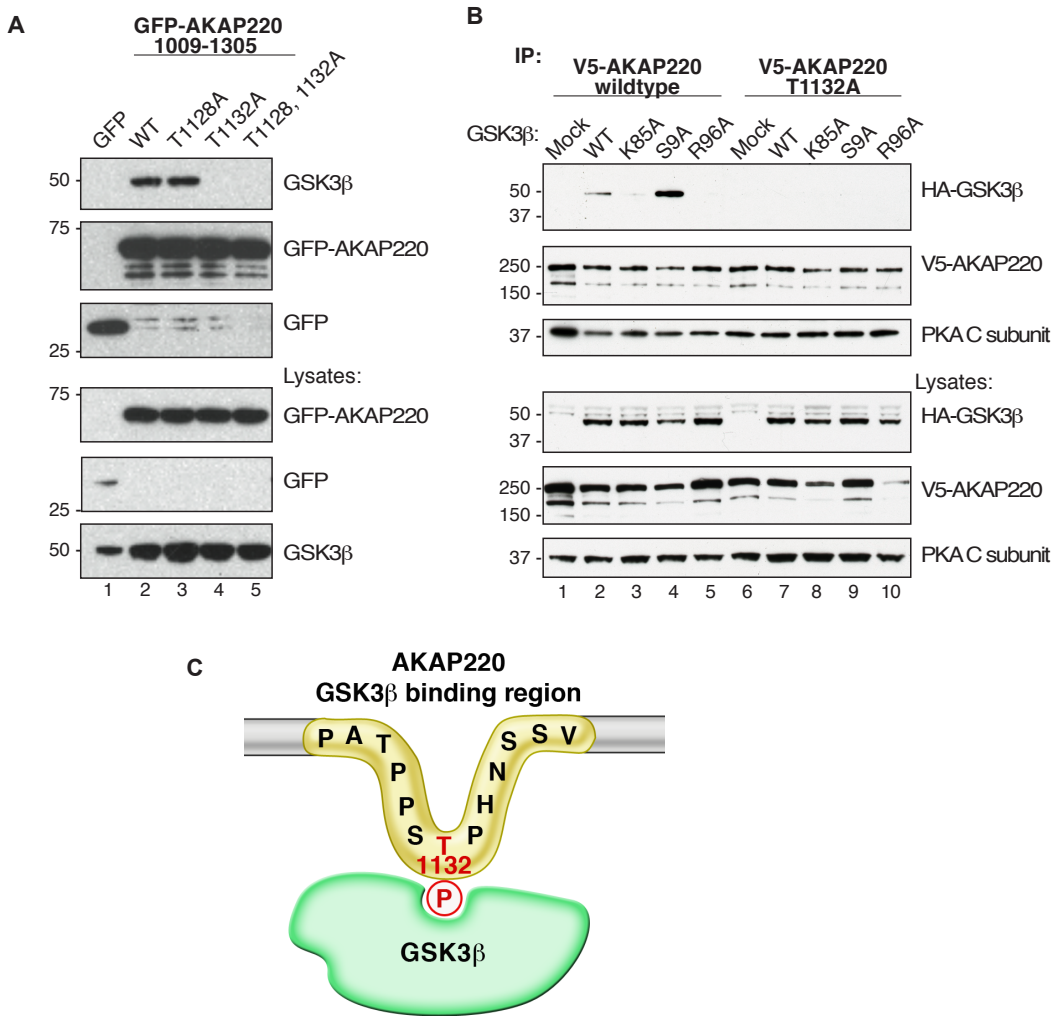

Figure 2.2: Active GSK3β interacts with AKAP220 at Thr1132. A) Lysates from cells expressing GFP-AKAP220 (1009-1305) wild-type, T1128A, T1132A, or the T1128, 1132A double mutant were immunoprecipitated with anti-GFP antibody. Co-precipitation of endogenous GSK3β was assessed by immunoblot with an anti-GFP antibody. B) Full length V5-AKAP220 wild-type or V5-AKAP220-T1132A were co-expressed in HEK293 cells with HA-GSK3β wild-type, HA-GSK3β-K85A, HA-GSK3β-S9A, or HA-GSK3β-R96A. Immunocomplexes were isolated with a V5-antibody and probed for HA-GSK3β by western blot. More GSK3β-S9A was detected compared to wild-type. GSK3β-K85A and R96A were not detected. No forms of GSK3β were detected in pulldowns using the AKAP220-T1132A mutant. C) Schematic representation of the AKAP220 Thr1132 phosphosite binding to active GSK3β.

AKAP220-GSK3β complexes are present in membrane ruffles

The subcellular location of AKAP220-GSK3β complexes was observed by immunofluorescence microscopy. HEK293 cells were transfected with full length YFP-AKAP220 and stained with antibodies against YFP (AKAP220) and endogenous GSK3β (Fig. 2.3A). Both proteins were enriched at membrane ruffles (identified by phalloidin f-actin staining) and were readily detected in the cytosol (Fig. 2.3A). These results are consistent with previous reports of AKAP220 localization in HT1080 cells, where it binds IQGAP1 and promotes actin polymerization in membrane ruffles [25].

For this reason, we next investigated whether AKAP220 may serve to anchor GSK3β near substrates in membrane ruffles. For this purpose, we selected an immortalized epithelial line produced from mouse inner medullary collecting ducts (mIMCD3). These cells were chosen for their high endogenous expression of AKAP220 and amenability to genome editing techniques. Using co-immunoprecipitation, we first confirmed that endogenous AKAP220 and GSK3β interact in the wild-type mIMCD3 cell line (Fig. 2.3B). Interestingly, we also detected endogenous β-catenin in AKAP220 immunocomplexes, a well-known downstream target of GSK3β (Fig. 2.3B).

Based on this information, we decided to produce an AKAP220-null cell line to gain further understanding of its function in membrane ruffles. Using CRISPR-Cas9 technology, the AKAP220$^{-/-}$ cell line was created using a synthetic guide RNA (sgRNA) that recognized the first coding exon of AKAP220 (Fig. 2.3C). Sequencing analysis of several clones revealed one clone with frame shift mutations and early stop-codons on both alleles of the *Akap11* gene (Fig. 2.3D). Complete loss of AKAP220 protein expression in the AKAP220$^{-/-}$ line was verified by western blot (Fig. 2.3E).

AKAP220 anchors both GSK3β and β-catenin in membrane ruffles

To visualize protein localization, mIMCD3 cells were grown on glass coverslips and stimulated with PDGF (50ng/ml for 30min) to induce membrane ruffling. The cells were fixed and stained with antibodies against endogenous GSK3β and β-catenin, and

membrane ruffles were identified by phalloidin staining for f-actin. In wild-type mIMCD3 cells, both GSK3β and β-catenin were enriched in membrane ruffles (Fig. 2.3F, arrowheads). Regions of distinct co-distribution were evident in these actin-rich structures (Fig. 2.3F, insets). As expected, loss of AKAP220 caused a re-distribution of GSK3β away from membrane ruffles (Fig. 2.3G). Interestingly, β-catenin was also lost from ruffles in AKAP220$^{-/-}$ cells (Fig. 2.3G, insets).

The distribution of β-catenin at the ruffle edge was quantified by line plot analysis of fluorescence intensity. In wild-type cells, β-catenin signal increased adjacent to the ruffle edge (Fig. 2.3H, gray line). In AKAP220$^{-/-}$ cells, however, the peak fluorescence intensity at the ruffle edge was significantly reduced (Fig. 2.3H, blue line). Comparison of β-catenin fluorescence intensity 1 μm from the plasma membrane confirmed a significant reduction in AKAP220$^{-/-}$ cells (average of n=3 experiments, ≥18 cells per experiment) (Fig. 2.3I). These functional studies in AKAP220$^{-/-}$ cells confirm that AKAP220 localizes GSK3β with its substrate β-catenin and recruits both proteins to membrane ruffles.

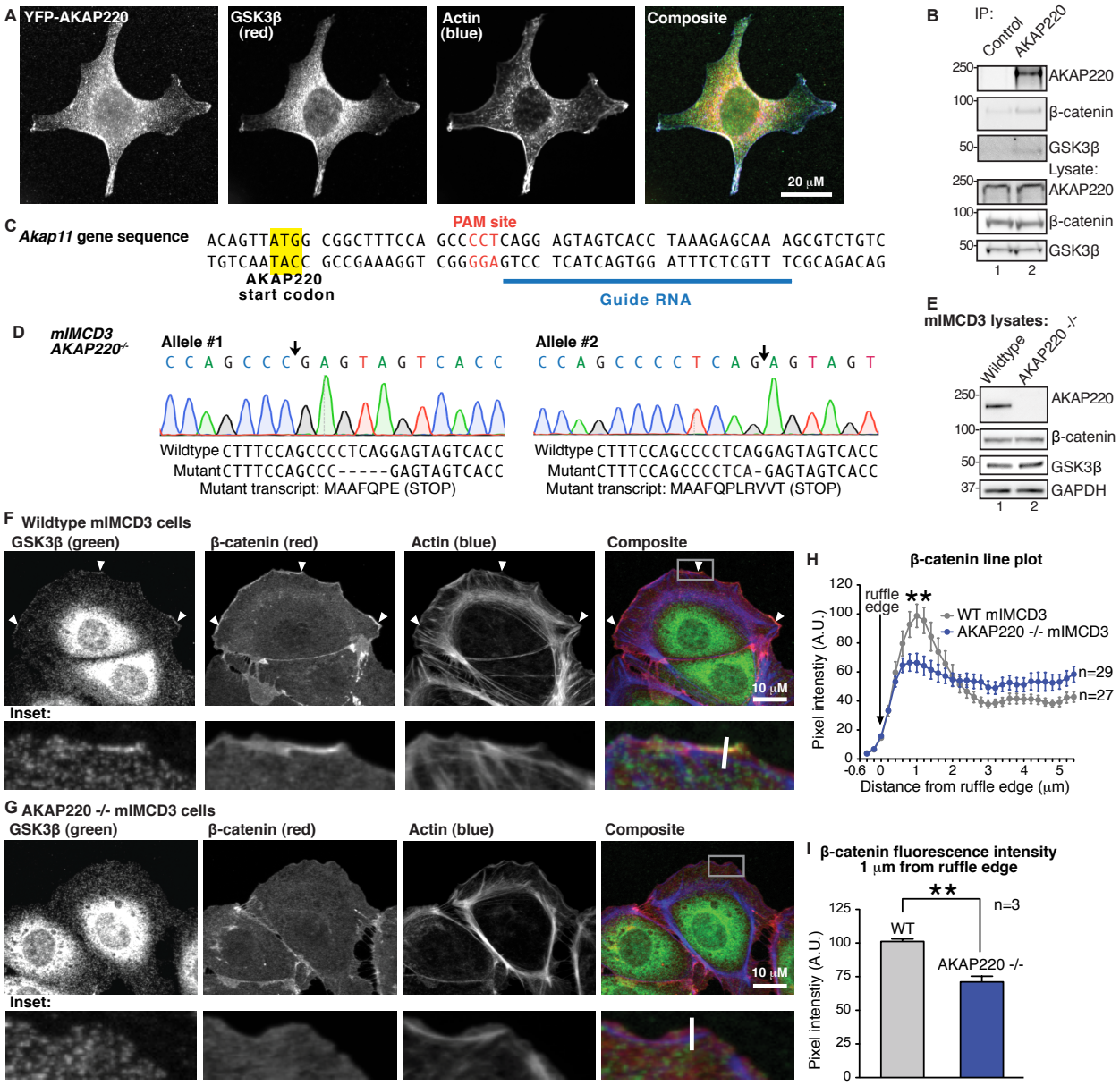

Figure 2.3: AKAP220 localizes GSK3β and β-catenin to membrane ruffles. A) HEK293 cell expressing YFP-AKAP220 were stained for YFP (AKAP220, green) endogenous GSK3β (red), and actin (phalloidin, blue). AKAP220 and GSK3β co-distribute in the cytosol and are both enriched in membrane ruffles. **B**) Co-immunoprecipitation of endogenous AKAP220 from wild-type mIMCD3 cells detected an interaction with GSK3β and β-catenin. **C**) CRISPR-Cas9 gene editing was used to disrupt the *Akap11* gene using the indicated sgRNA. **D**) Sequencing analysis of the AKAP220$^{-/-}$ clone demonstrates deletions on both *Akap11* alleles (site of deletion indicated by black arrows). The wild-type and mutant sequences are listed, with the resulting mutant transcripts from each allele indicated. Both mutations create early in-frame stop codons. **E**) Complete loss of AKAP220 protein expression was confirmed by western blot. **F**) Wild-type and AKAP220$^{-/-}$ mIMCD3 cells were stained for endogenous GSK3β (green), β-catenin (red), and f-actin (phalloidin, blue). Membrane ruffles were

identified as regions with positive f-actin stain. The location of zoomed insets is indicated (white boxes). In wild-type cells, both GSK3β and β-catenin were enriched in ruffles (arrowheads). **G**) No GSK3β or β-catenin enrichment was observed in membrane ruffles of AKAP220 -/- cells. **H**) Representative quantification of β-catenin distribution at the membrane from one experiment. Fluorescence intensity was measured by line plot analysis, with lines drawn perpendicular to the ruffle edge (representative white lines indicated on insets). I) Average β-catenin fluorescence intensity 1 μm from the ruffle edge was significantly reduced in AKAP220-/- cells (average of n=3 experiments, >18 cells per condition per experiment).

Identification of a novel PKA anchoring site on AKAP220

The initial discovery and characterization of AKAP220 mapped an R subunit-binding site corresponding to residues 1633-1646 in the mouse protein [22]. However, deleting this fourteen amino acid segment did not eliminate all PKA association with AKAP220 (Fig 2.4A). HEK293 cells were transfected with wild-type AKAP220 or AKAP220 Δ1633-1646. As expected, the C subunit of PKA co-fractionated with wild-type AKAP220, but it also co-fractionated with the mutant form. Therefore we concluded that AKAP220 contains at least one additional PKA-anchoring site that had not yet been identified.

We used a complementary pulldown approach to map the location of the novel PKA-binding site. HEK293 cells were transfected with flag-tagged constructs encoding the N-terminal (1-1015) or C-terminal (1009-1894) halves of the anchoring protein (Fig. 2.4B). AKAP220 complexes were co-purified by virtue of the R subunit affinity for cAMP-agarose. As expected, the C-terminal half of AKAP220 (containing the known PKA site) was readily detected by immunoblot (Fig. 2.4C, lane 3). However, the N-terminal half of AKAP220 was also detected, and must therefore contain a PKA-binding site (Fig. 2.4C, lane 2).

Next, immunofluorescence microscopy was used to visualize the subcellular distribution of AKAP220 and fragments with RII inside cells. Transfected HEK293 cells fixed in 4% paraformaldehyde were stained for AKAP220 and fragments (anti-flag; green) and endogenous RII subunit of PKA (anti-RII; red). Each AKAP220 form had distinct

cytosolic and peri-nuclear co-distribution with RII (Fig. 2.4 D-F). Taken together, these biochemical and cell-based experiments support our hypothesis that at least one additional PKA-binding site resides within the first 1015 residues of AKAP220.

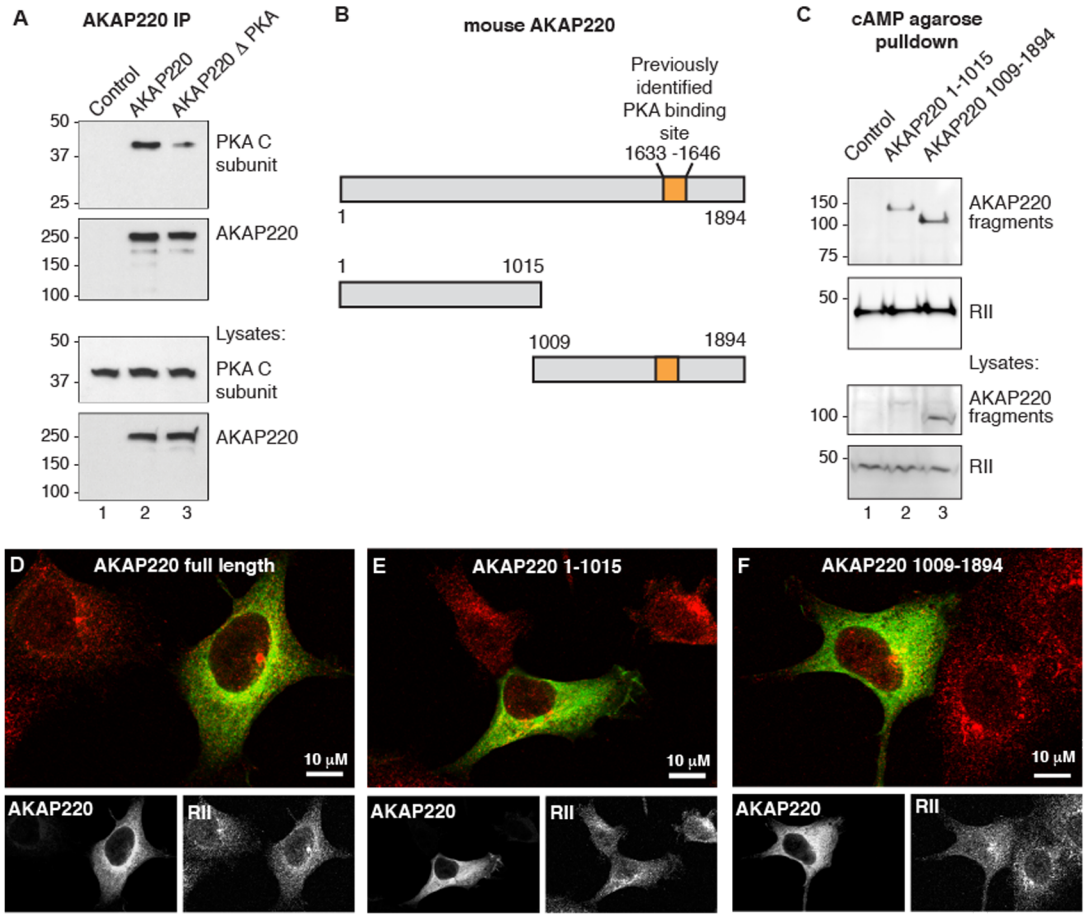

Figure 2.4 – Identification of a novel PKA interaction in the N-terminal region of AKAP220. A) Deletion of the known PKA-binding site (residues 1633-1646) did not abolish the interaction with PKA, as assessed by co-IP and immunoblot. B) Schematic representation of full length AKAP220 and the N-terminal (1-1015) and C-terminal (1009-1894) fragments. C) Both fragments were detected by cAMP agarose pulldown, indicating the ability to bind R subunit. D) Expression of each construct in HEK293 cells demonstrated regions of co-distribution with endogenous R subunit.

To locate the novel binding site, we searched for prospective candidates between AKAP220 residues 1-1015. Structural approaches have shown that the hydrophobic face of an amphipathic helix on AKAPs interacts with the PKA regulatory (R) subunit [38,39]. Algorithms have been developed to screen for prospective R subunit anchoring helices [10,40]. Although R subunit anchoring sites are not strictly conserved at the amino acid sequence level, the binding motif is typically 14-18 amino acids and forms an amphipathic helix. When folded, this helix creates a suitable hydrophobic surface that interfaces with the docking and dimerization domain of the R subunit. Using these known principles, residues 610-623 of AKAP220 were predicted to be a putative PKA binding site (Fig. 2.5A-B). This region is almost invariant in mammalian orthologs of AKAP220, and it also resembles the previously defined PKA-binding helix on AKAP220 and other AKAPs (Fig. 2.5C).

To test the PKA binding capacity of this newly identified region, cAMP agarose pulldowns were conducted with wild-type and helix-deletion mutants of AKAP220 (Fig 2.5D). These constructs were full-length AKAP220, AKAP220 Δ site 1 (Δ610-623), AKAP220 Δ site 2 (Δ1633-1646), and AKAP220 double delete (Δ610-623, Δ1633-1646). Full-length AKAP220 and each single-deletion helix mutant were detected in these pulldowns. In contrast, the double- deletion mutant was not detected (Fig. 2.5D). This demonstrates that each binding helix on AKAP220 is sufficient for interaction with the PKA R subunit, and that removal of both helical regions completely abolishes binding. These experiments establish the presence of two PKA-binding sites on AKAP220 that are capable of independent interaction with the PKA holoenzyme.

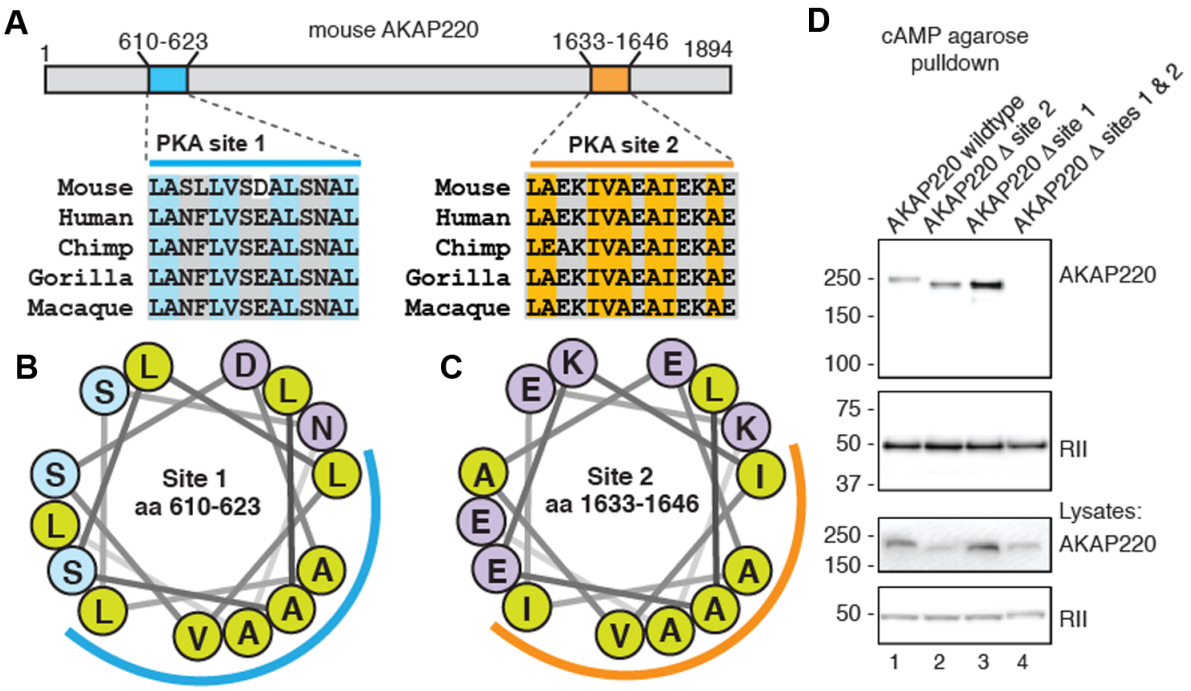

Figure 2.5 – Identification and mapping of a novel PKA binding site on AKAP220. A) Schematic representation of the known PKA binding site between residues 1633-1646 (orange) and the predicted site between residues 610-633 (blue). The amino acid sequences are conserved in species and resemble typical PKA anchoring motifs. B-C) Helical wheel predictions for these binding sites demonstrate their capacity to form a hydrophobic surface suitable for R subunit binding. D) Helix deletion constructs were subjected to cAMP pulldown analysis. Single deletion of either site did not eliminate PKA binding, indicating each site is sufficient for anchoring PKA to AKAP220. However, deletion of both helical segments completely eliminated the interaction and suggests there are no additional PKA binding sites on AKAP220.

The PKA binding sites on AKAP220 have differential isoform selectivity

Although most AKAPs preferentially bind type II PKA, a few type I-selective AKAPs have also been reported [41,42]. Another subset, designated dual function AKAPs, can interact with either RI or RII. We evaluated each PKA-binding helix to characterize the overall isoform preferences for AKAP220. To do this, his-tagged MBP-fusion proteins encompassing each PKA-binding site were expressed in *E. coli* and purified on a nickel-NTA column (Fig. 2.6A). Both of these fragments bound RII as detected by biotin-RII

overlay. However, only site 2 was detected by biotin-RI overlay. These initial findings suggested that AKAP220 site 1 is RII-selective while site 2 has dual-specificity for RI and RII.

AKAP220 peptides encompassing each binding site were then synthesized onto a cellulose membrane by peptide array (Fig. 2.6 B-C). Super-AKAP*is* and RIAD peptides were used as positive controls for RII and RI binding, respectively [8,43]. As negative binding controls, helix-disrupting proline mutations were introduced into each peptide sequence. As anticipated, both the AKAP220 site 1 and site 2 peptides were detected by biotin-RII overlay. This signal was completely abolished in proline mutant forms, indicating the formation of an amphipathic helix was required for RII binding. Only the AKAP220 site 2 peptide was detected by biotin-RI overlay. These data support that site 2 has dual-specific PKA binding capacity, while site 1 binds only to RII (Fig. 2.6E).

We next used fluorescence polarization experiments to measure the apparent binding affinities of the AKAP peptides for RII. FITC-conjugated peptides (22mers) encompassing site 1 or site 2 of AKAP220 were synthesized. FITC-AKAP*is* served as a positive control, and the scrambled sequence as a negative control. Increasing concentrations of purified RIIα (50 pM to 5 μM) were added to a fixed concentration of each FITC peptide (5 nM). Binding equilibrium was reached after a 30-minute incubation at room temperature, and the fluorescence polarization was measured with a plate reader (Fig. 2.6H).

Using this approach, the dissociation constant (Kd) for RIIα and the site 2 peptide was measured at 36.5 +/- 9.3 nM. This value was comparable to AKAP*is* at 26.1 +/- 4.2 nM. In contrast, the Kd for site 2 was almost 10-fold lower, at 250.5 +/- 10.1 nM (Fig. 2.6H). The scrambled peptide did not bind RII. These measurements support and explain the differences in signal strength seen in Figure 6D. We attempted to repeat this assay with RI, but were unable to reach saturation and therefore could not calculate binding affinities. Together, the data in Figure 3 determines that site 1 (residues 610-623) of AKAP220 is RII-selective, whereas site 2 (residues 1633-1646) is a dual specificity PKA-anchoring site.

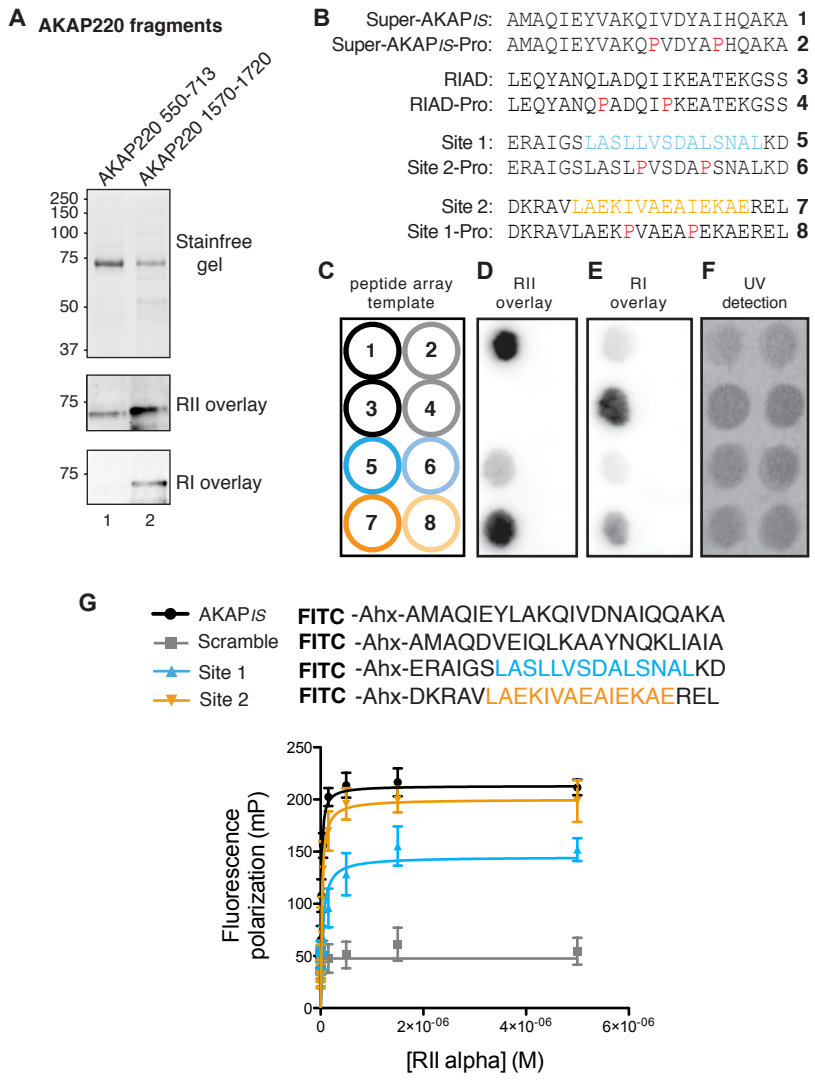

Figure 2.6 – Characterization of isoform-specific PKA binding to AKAP220 A) AKAP220 fragments encompassing site 1 (550-713) and site 2 (1570-1720) were expressed as His- MBP fusion proteins *E. coli*. Purity and loading was verified by stain-free gel. R-subunit overlays detected isoform-specific binding characteristics of each fragment. B) The amino acid sequences of peptides synthesized in peptide arrays (C-F) are shown for PKA-binding site 1 and site 2. Super-AKAP*is* and RIAD were used as positive controls for RII and RI binding, respectively. Negative binding controls incorporated helix-disrupting proline substitutions (red). C) Schematic of the peptide array layout. D) Biotin-RII overlay detected binding to Super-AKAP*is* and AKAP220 site 2. A weak signal was detected for AKAP220 site 1. No signal was detected for RIAD or any of the proline mutant peptides. E) Overlay with biotin-RI detected RIAD and AKAP220 site 2. No signal was detected for AKAP220 site 1, Super-AKAP*is*, or any of the proline mutant peptides. F) Spotting efficiency confirmed by UV. G) FITC-conjugated peptide sequences used to determine RII-binding affinity measurements by fluorescence polarization. H) Saturation binding experiments determined the binding affinity of each peptide for RIIα.

AKAP220 interacts with type I and type II PKA in situ

To examine AKAP220 interaction with type I and type II PKA in cells, we used a proximity ligation assay (PLA). This *in situ* approach uses two secondary antibody probes conjugated to DNA oligonucleotides[44]. Enzymatic ligation and rolling circle DNA amplification occurs only when both probes bind their targets within 40-60nm of each other. Subsequent *in situ* hybridization of fluorescently tagged complementary oligonucleotides generates fluorescent puncta visible by microscope. Detection of these PLA puncta denotes the location and abundance of individual AKAP220-R subunit pairs.

HEK293 cells were transfected with the full-length AKAP220 or the N-terminal (1-1015) or C-terminal (1009-1894) fragments described previously. As a control, cells expressing full length AKAP220 were treated with the anchoring inhibitor peptide Ht31 to universally disrupt R subunit-AKAP interactions [18]. Cells were fixed and incubated with antibodies for endogenous RI or RII and AKAP220 (anti-flag). Following the proximity ligation reaction cells were counterstained with FITC-anti-flag to detect transfected cells. Maximum projection images were collected by laser scanning confocal microscopy and PLA puncta were quantified by semi-automatic analysis as described previously [44]. Cells that were positive for FITC anti-flag stain were delineated by hand for analysis. PLA signal was defined as local intensity maxima above a background threshold, and measured with the Find Maxima algorithm in ImageJ.

As expected, PLA signal was detected between full length AKAP220 and endogenous RII (Fig. 7A). A comparable number of PLA puncta were counted for both the site 1 and site 2 AKAP220 fragments, verifying that each fragment effectively binds RII inside cells (Fig. 2.7C). Treatment with Ht31 reduced the number of puncta, confirming the fidelity of the assay (Fig. 7G). The total number of puncta per cell was quantified for n=50 cells per condition (Fig. 2.7Q).

Parallel experiments also detected an interaction between full length AKAP220 and RI in cells (Fig. 2.7I). The number of puncta for the AKAP220 site 2 fragment was comparable to wild-type, confirming this site has dual-specific R subunit binding capacity (Fig. 2.7K). However, the AKAP220 site 1 fragment had reduced PLA signal

comparable to that seen in Ht31-treated cells (Fig. 2.7M). The total number of puncta per cell was quantified for n=50 cells per condition (Fig. 2.7R). These results further support that AKAP220 site 2 (residues 1633-1646) can bind RI or RII while site 1 (residues 610-623) is RII-selective.

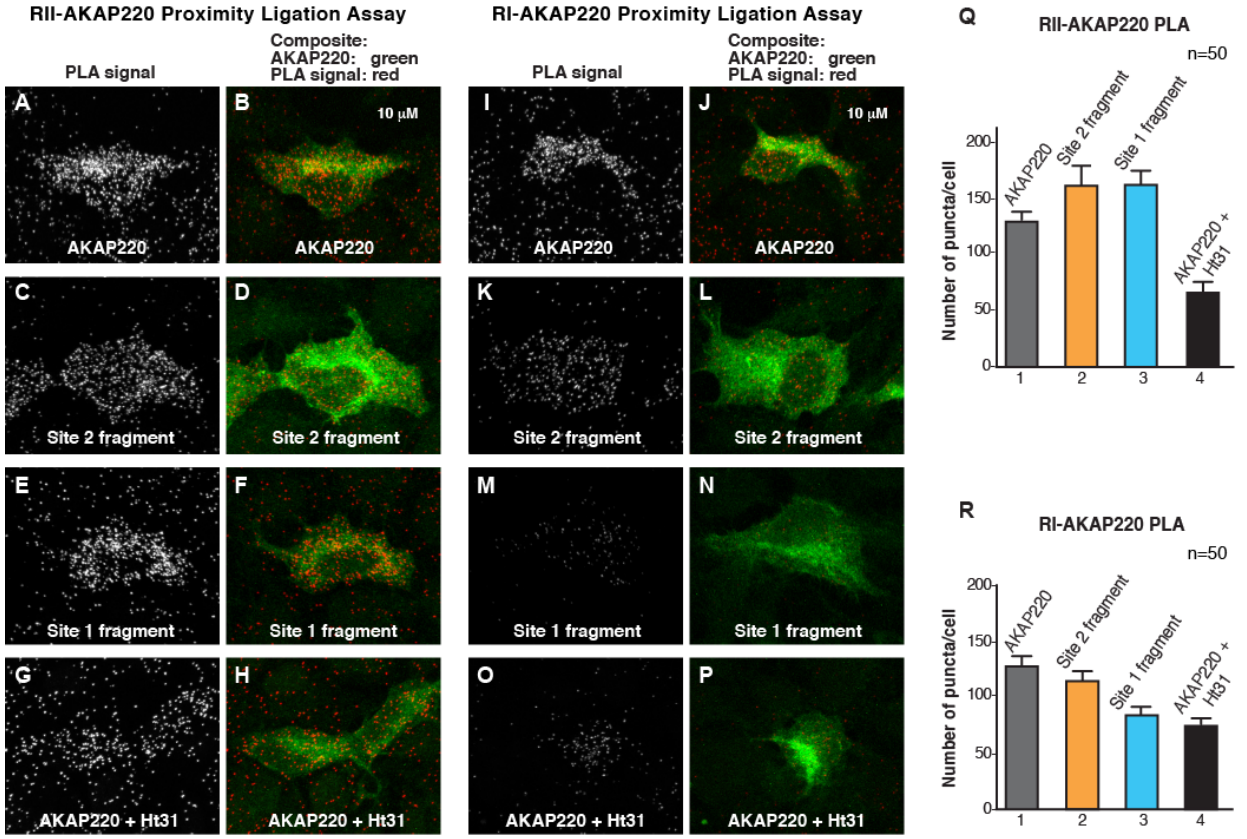

Figure 2.7 – AKAP220 interacts with type I and type II PKA in cells. A-H) A Proximity Ligation Assay (PLA) was used to detect protein-protein interactions between AKAP220 and RII inside intact HEK293 cells. PLA signal between RII and the wild-type, N- and C-terminal fragments of AKAP220 is seen as puncta (red). Transfected cells were identified by FITC anti-flag counterstain (green). Treatment with the R subunit anchoring inhibitor peptide Ht31 was used to disrupt the interaction. I-P) The PLA assay was repeated between RI and the AKAP220 fragments. PLA signal was detected between RI and the wild-type and C-terminal fragment, but was reduced with the N-terminal fragment (red). Transfected cells were identified by FITC anti-flag counterstain (green). The interaction with RI was disrupted when Ht31 was present. Q-R) Quantification of total PLA puncta per cell (n=50 cells per condition) for each experiment.

Anchored PKA modulates GSK3β binding to AKAP220

PKA phosphorylation of GSK3β at serine 9 suppresses enzyme activity [36]. Therefore, we assessed whether crosstalk between these kinases could influence AKAP220 complex assembly. HEK293 cells were transfected with wild-type AKAP220 and stimulated with 10 μM forskolin and 75 μM IBMX (FSK/IBMX) to increase intracellular cAMP. This treatment decreased GSK3β pulldown with AKAP220 complexes compared to basal conditions, suggesting that GSK3β dissociates from AKAP220 in response to PKA activation (Fig. 2.8).

To determine whether PKA anchored within the complex mediated this effect the experiment was repeated with an AKAP220 mutant lacking both PKA binding helices (AKAP220-Δsite1-Δsite2). In this context, GSK3β dissociation in response to FSK/IBMX was blunted (Fig. 2.8B). Therefore, we conclude that an anchored pool of PKA primarily controls this dissociation event. We confirmed that phospho-GSK3β levels in the cell lysates increased following FSK/IBMX stimulation. Taken together these experiments demonstrate that AKAP220 complexes are dynamic and that anchored PKA can oppose the recruitment of GSK3β in response to signal transduction events.

Schematic representations of the AKAP220 signaling complex are presented (Fig. 2.8C-D). The precisely mapped binding sites for GSK3β, PKA, and PP1 are indicated. The two PKA binding sites have differential isoform specificity, with site 1 being RII-selective and site 2 having dual-specificity for both RI and RII. GSK3β phosphorylates Thr1132 to both create and maintain its binding site, which can be opposed by cAMP activation of anchored PKA within the complex.

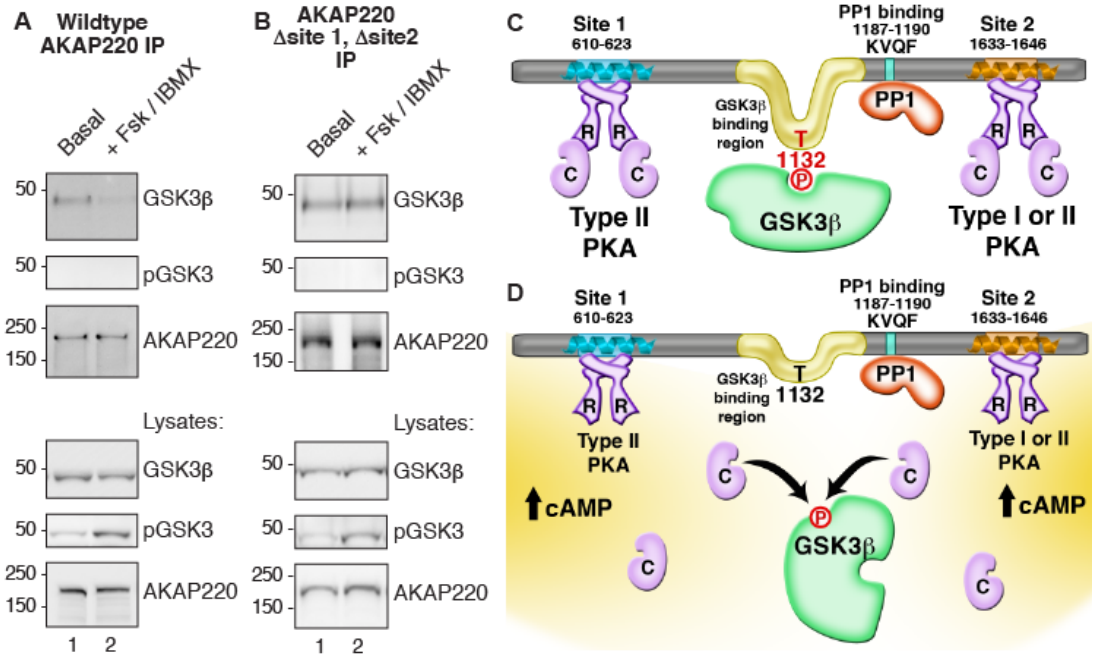

Figure 2.8 – GSK3β dissociates from AKAP220 complexes in response to cAMP. A) HEK293 cells were stimulated with 10 μM FSK and 75 μM IBMX for 10 min at 37 ˚C to increase intracellular cAMP and activate PKA. GSK3β pulldown with AKAP220 was decreased in stimulated cells. An antibody specific for phospho-GSK3β-Ser9 detected higher signal in the treated lysates, confirming stimulation. No phospho-GSK3β-Ser9 was detected in the pulldowns. B) The experiment was repeated with a mutant form of AKAP220 that does not bind PKA. Dissociation of GSK3β was blunted in these conditions. C) Schematic representation of enzyme binding sites on AKAP220. PKA can bind to two sites. Site 1 is RII-selective, and site 2 has dual-specificity for RI or RII. One copy of active GSK3β interacts with AKAP220 between residues 1126-1145, a region containing the GSK3β phosphosite at Thr1132 that is required for GSK3β binding. Additionally, PP1 binds to the KVQF motif at residues 1187-1190. **D)** Proposed model of cAMP responsive GSK3β dissociation from AKAP220. In response to cAMP, anchored PKA is activated and the C subunits are released. Anchored GSK3β is phosphorylated, preventing it from phosphorylating Thr1132 causing its release from the complex. Anchored PP1 may relieve PKA-mediated inhibition of GSK3β by dephosphorylating Ser9, providing bi-directional control of AKAP220 complex formation in response to cAMP.

Discussion

AKAPs utilize various mechanisms to exert dynamic and local control of signal transduction events. The predominant mechanistic theme emerging from this study is that AKAP220 crosstalk between PKA and GSK3β is augmented by AKAP220. Specifically, PKA negatively regulates local GSK3β activity and binding to the signaling complex in response to cAMP.

The findings presented here also place AKAP220 among a select group of AKAPs with the capacity to sequester multiple PKA holoenzymes. For example, the multivalent scaffolding protein yotiao/AKAP450 contains two PKA binding sites and constrains a range of protein kinases and phosphatases at the golgi and centrosomes[45,46]. Likewise, the sphingosine kinase interacting protein (SKIP) is an RI-selective anchoring protein that tethers a pair of type I PKA holoenzymes with preferred substrates at the inner face of the mitochondrial matrix[41,47].

Our work also demonstrates that the PKA-binding sites on AKAP220 have differential PKA isoform selectivity. Site 1 on AKAP220 (residues 610-623) is RII-selective, while site 2 (1633-1646) exhibits a dual specificity for RI and RII. It is possible that AKAP220 anchors distinct PKA isoforms to target different downstream substrates. This is particularly relevant since RI and RII have different sensitivities to cAMP and also exhibit tissue specific and developmentally regulated patterns of expression. Possessing the ability to bind different R subunit isoforms likely ensures that AKAP220 has the ability to anchor PKA in a variety of cellular contexts. As AKAP220 is ubiquitously expressed, this scaffold has the potential to regulate diverse signaling events in different cell types and tissues. Such inherent flexibility in the PKA-binding profile of AKAP220 likely accommodates for such variable cellular environments.

In addition, it is interesting to note that most AKAPs have a higher affinity for RII than RI. The literature in this field generally supports the view that AKAPs anchor type II PKA, while type I PKA is more typically in a soluble, un-anchored form. However, we readily observed RI-binding to AKAP220 site 2 inside cells by proximity ligation assay. These findings indicate that although RI has a lower affinity for AKAP220 site 2, it can still successfully compete for binding in a cellular context. Therefore, we propose that

AKAP220 constrains a range of macromolecular complexes that include either type I or type II PKA.

Mechanistically, this could impact the duration of cAMP responses in the vicinity of AKAP220, particularly because type I PKA is more sensitive to cAMP than type II PKA [48,49]. Additionally, such responses may be more robust if two PKA holoenzymes are simultaneously anchored by AKAP220. An illustrative example of this concept comes from evidence that SKIP complexes exist in different states of RI-occupancy [47]. The experimental approaches utilized in these studies unfortunately do not allow us to assess simultaneous binding site occupancy. Further experiments are needed to investigate the stoichiometry of AKAP220-PKA complexes, perhaps using multi-angle light scattering (MALS) to measure the molecular weights of different purified AKAP220 and R subunit complexes. Alternatively, these macromolecular complexes could be explored directly from cell or tissue extracts using the single molecule pulldown (SiMPull) approach.

One biological role for PKA anchored by AKAP220 is to ensure the compartmentalized regulation of local GSK3β. Unlike most serine/threonine protein kinases, GSK3β is active under basal conditions. As previously stated, suppression of GSK3β activity occurs upon phosphorylation of serine 9 by upstream kinases including PKA and Akt. In this report we show that AKAP220-associated PKA contributes to the phosphorylation-dependent modulation of GSK3β, in part because both enzymes reside within the same macromolecular complex. Our work further indicates that AKAP220 preferentially sequesters catalytically active GSK3β. We show that the constitutively active GSK3β-S9A mutant has enhanced binding to AKAP220, whereas neither the kinase-dead GSK3β-K85A nor the phosphate binding site mutant GSK3β-R96A were able to bind.

A previous study demonstrated binding between a C-terminal AKAP220 fragment (residues 1011-1901) and two catalytically inactive forms of GSK3β, H85M and Y216F[23]. The conflicting results in these studies may be due to varied degree of kinase inhibition or conformational differences between the GSK3β-H85M and Y216F mutants used in the previous work and the K85A and R96A mutant forms used here. Additionally, our studies utilized full-length AKAP220 rather than a truncated fragment of the anchoring

protein. Thus, secondary contact points on AKAP220 may be involved in modulating the interaction with catalytically active GSK3β. Future structural analyses of the binding interface on GSK3β may ultimately provide details to resolve these outstanding questions. The previous work had also demonstrated that cAMP stimulation reduced the GSK3β activity on AKAP220 complexes through activation of anchored PKA. However, these studies did not investigate GSK3β following stimulation. These studies concluded that the observed decrease in GSK3β kinase activity in the complex was due to phospho-dependent inhibition by PKA. However, our work adds new insight to this mechanism, suggesting that not only does PKA inhibit GSK3β but it also promotes complete dissociation from the complex. This, too, would explain the previously observed decrease in associated kinase activity and adds further information to our understanding of AKAP220 signaling complexes.

The preferential association of catalytically active GSK3β with AKAP220 is further underscored by our identification of AKAP220-Thr1132 as a phosphosite that is required for GSK3β recruitment. Substituting Thr1132 with alanine abolishes GSK3β binding, emphasizing a role for the phosphate moiety as a molecular determinant of GSK3β anchoring. Our findings can be consolidated into a mechanism presented in Figure 2.8C, whereby catalytically active GSK3β is required to both establish and maintain the interaction with AKAP220 by phosphorylating Thr1132 on the anchoring protein.

It has long been recognized that GSK3 has a preference for "primed" or pre-phosphorylated substrates, although under certain conditions it is not required [28]. This is consistent with our *in vitro* kinase assay experiment showing Thr1132 on AKAP220 is phosphorylated by GSK3β even in the absence of a priming phosphate at the n+4 position. However, we also note Ser1136 on the anchoring protein is optimally positioned to serve as such a priming site, and may be a substrate for a different kinase in a cellular context. Another interesting possibility is that phosphorylation of Thr1132 may initiate the processive phosphorylation of another consensus GSK3β site located four residues upstream at Thr1128. We noted that a single alanine substitution at Thr1132 reduced but did not entirely eliminate peptide phosphorylation by *in vitro* kinase assay (Fig. 2.1D). GSK3β-mediated priming of Thr1132 may serve as a prerequisite for efficient phosphorylation of Thr1128. Taken together, these findings underscore the

importance of phospho-Thr1132 as a primary determinant for recruitment of active GSK3β to the AKAP220 signaling scaffold.

The significance of GSK3β anchoring is emphasized by the discovery that AKAP220 interacts with β-catenin, a well-known GSK3β substrate. In fact, AKAP220 is involved in localizing both GSK3β and β-catenin to membrane ruffles, as our quantitative image analysis shows deficient enrichment of GSK3β or β-catenin at the ruffle edge in AKAP220$^{-/-}$ cells. These results suggest that AKAP220 may facilitate signaling between these two proteins during lamellipodia and ruffle formation. These new observations are consistent with work by our lab demonstrating that siRNA-mediated knockdown of AKAP220 reduced membrane ruffling and slowed cell migration. These phenotypes were linked to the interaction between AKAP220 and IQGAP1, a known β-catenin binding partner. This large macro-molecular complex therefore contains several signaling components implicated in ruffling and migration that are recruited to the appropriate cellular location by AKAP220.

Another important facet of this study is the discovery that anchored PKA modulates the interaction between GSK3β and AKAP220. Our cell-based studies infer that cAMP stimulation promotes GSK3β dissociation from AKAP220 complexes. Importantly this effect is not observed with an AKAP220 mutant that is unable to anchor PKA. This finding raises interesting questions about crosstalk between these and other enzyme-binding partners. This is particularly relevant as AKAP220 also targets the catalytic subunit of the protein phosphatase PP1, an enzyme that may allow for bi-directional regulation of phosphorylation events. For example, inhibition of GSK3β via PKA-mediated phosphorylation of Ser9 can be relieved by PP1 dephosphorylation [50]. It is also possible that Thr1132 on AKAP220 is a prospective PP1 substrate. Because dephosphorylation of this residue could enhance GSK3β dissociation from the complex, PP1 may act cooperatively with PKA to strengthen the cAMP-mediated response. These ideas have been consolidated into a schematic that emphasize the major findings of this study, presented in Figure 2.8 C-D.

In conclusion we show that GSK3β binding to AKAP220 is regulated at multiple levels. First, GSK3β activity is required to phosphorylate Thr1132 on AKAP220. This

phosphorylation event both establishes and maintains the GSK3β-AKAP220 complex. Second, activation of AKAP220-associated PKA promotes GSK3β dissociation, likely through phosphorylation dependent inhibition of GSK3β activity. Finally, tethering of either type I or type II PKA holoenzymes may alter the magnitude and duration of the local cAMP response, as well as downstream substrates. The presence of two independent R subunit-anchoring helices on AKAP220 may represent a mechanism to amplify local cAMP responses, especially if two PKA holoenzymes can be simultaneously anchored. Our findings highlight the diverse and dynamic assembly of AKAP220 signaling complexes and demonstrate the utility of anchored enzyme crosstalk.

Chapter 3

Design and production of an AKAP220 knockout mouse

Introduction

Model organisms are invaluable tools for biomedical research. Different organisms are utilized for various research applications, depending on the biological questions being asked. Because the primary goal of biomedical research is to advance human health, a mammalian model is often desirable. Mice are commonly used in research labs because they are small, reproduce quickly, and have a relatively short lifespan. Because the mouse genome is ~95% similar to humans[51], this species provides a cost-effective research platform for studying many biological processes including growth and development, hormonal regulation, drug metabolism, and disease pathology[52]. Our lab combines the power of mouse genetics and genetic engineering to study the phenotypic effects of AKAP knockout or "knock-in" mutant mice.

For this work, we designed and produced a conditional knockout mouse model to help elucidate the biological significance of AKAP220. This 220kD protein, encoded by the *Akap11* gene, is evolutionarily conserved in mammals. We used the Cre-lox system to delete Exon 6 and Exon 7 from the mouse *Akap11* gene, representing 83% of the coding sequence and resulting in complete loss of AKAP220 expression. For this work, we designed the knockout and genetic engineering strategies and worked in collaboration with Vega Biolabs and the University of Washington Transgenic Resources Program to create the mouse line to our desired specifications.

Results

Knockout vector design

The knockout vector contained approximately 14kb of the C57Bl/6J genomic *Akap11* sequence surrounding Exons 6 and 7 (Fig. 3.1). A Neo cassette was engineered into Intron 5-6 to serve as a positive selection marker. This cassette was flanked with Frt sites so that it could be removed at a later stage by crossing to mice expressing FLP recombinase. Both the Neo cassette and the target sequence (Exons 6 and 7) were flanked with intronic loxP sites. Cre-mediated combination of these loxP sites would eliminate 83% of the coding sequence for *Akap11*, and the remaining exons are all out of frame with the exception of exon 12. This minimizes the possibility of residual expression of AKAP220 splice variants.

The knockout vector also contained a TK cassette for negative selection of clones with incomplete recombination. Because recombination at the target site is less likely than random vector insertion, the TK cassette helps eliminate false positives. Finally, a unique restriction site for the enzyme I-CeuI was included for vector linearization prior to electroporation in the embryonic stem cells.

To simplify Southern blot screening for homologous recombination, we took advantage of naturally occurring BamHI and StuI sites within the *Akap11* genomic sequence. We added a new BamHI site adjacent to the Neo cassette and a new StuI site adjacent to the downstream loxP. The Southern blot was designed to distinguish homologous recombination events at both the 5’ and 3’ arms of the target sequence.

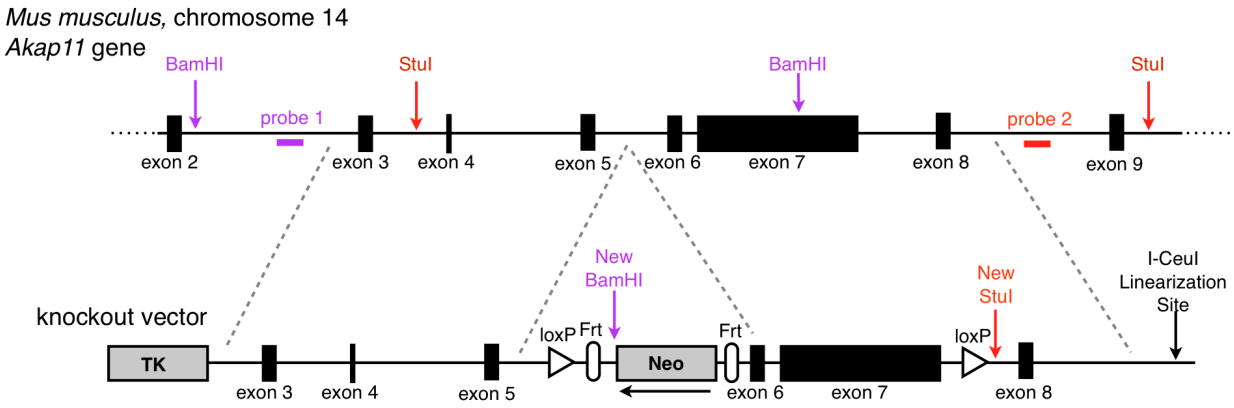

Figure 3.1: Schematic representation of the *Akap11* knockout vector. The vector backbone contained approximately 14 kilobases of the genomic *Akap11* sequence flanking the target sequence (Exons 6 and 7). The neomycin gene (Neo) was inserted upstream of Exon 6 to allow for G418 screening of embryonic stem cells. This Neo cassette was flanked with Frt sites for later removal by FLP recombinase. The 5' loxP site was inserted upstream of the Neo cassette and the 3' loxP site was downstream of Exon 7. To simplify Southern blot screening, new cut sites for BamHI (purple) and StuI (red) were engineered into the knockout vector. The Southern blot probes were generated by PCR from the indicated regions of *Akap11* genomic DNA.

Screening stem cell clones

The knockout vector was purified and linearized with the I-CeuI restriction enzyme. This linearized DNA was given to the University of Washington Transgenics Resources Core, where it was electroporated into G4 hybrid mouse embryonic stem cells (ES cells). Clones were grown and expanded in the presence of G418 for positive selection. DNA was harvested from 96 samples for initial PCR-based screening. Of these, 22% tested positive for the 3' loxP site (21 out of 96 clones) and were further analyzed by Southern Blot. Successful homologous recombination of both the 5' and 3' arms was confirmed in ES clones #42 and #70 (Fig. 3.2 A-B). The recombination was confirmed to be restricted to only one *Akap11* allele, as both the wild-type (13.0kb) and recombined (8.3kb) bands were detected, indicating *Akap11* heterozygosity. Interestingly, the StuI

probe detected two wild-type bands from the G4 hybrid stem cells. It is possible that a genetic polymorphism in the 129S6 genomic background generates an additional StuI cut site in *Akap11* and results in a band at the observed size with our probe. Because the knockout vector was produced with C57Bl/6J genomic sequence, the loss of the expected wild-type band (18.4kb) indicates that the recombination event occurred on this allele. Correspondingly, two bands were detected at the expected sizes for the recombined allele (9.3kb) and the apparent 129S6 wild-type allele (~17kb) for the heterozygous ES clones #42 and #70.

These ES clones were expanded and microinjected into C57Bl/6 blastocysts by the UW Transgenics Resources Program. Chimeric offspring were identified by agouti coat color conferred by the G4 ES cell line. Three chimeric mice were obtained. ES clone 42 produced a 99% agouti male and a 100% agouti female, and ES clone 70 produced a single 100% agouti male. These mice were bred to wild-type C57Bl/6J mice to confirm germline transmission of the floxed *Akap11* allele. The male chimera from ES clone 42 was sterile, and the female only produced wild-type offspring. The male chimera from ES clone 70, however, had successful germline transmission and the floxed allele was readily detected by PCR analysis (Fig 3.2 C-E).

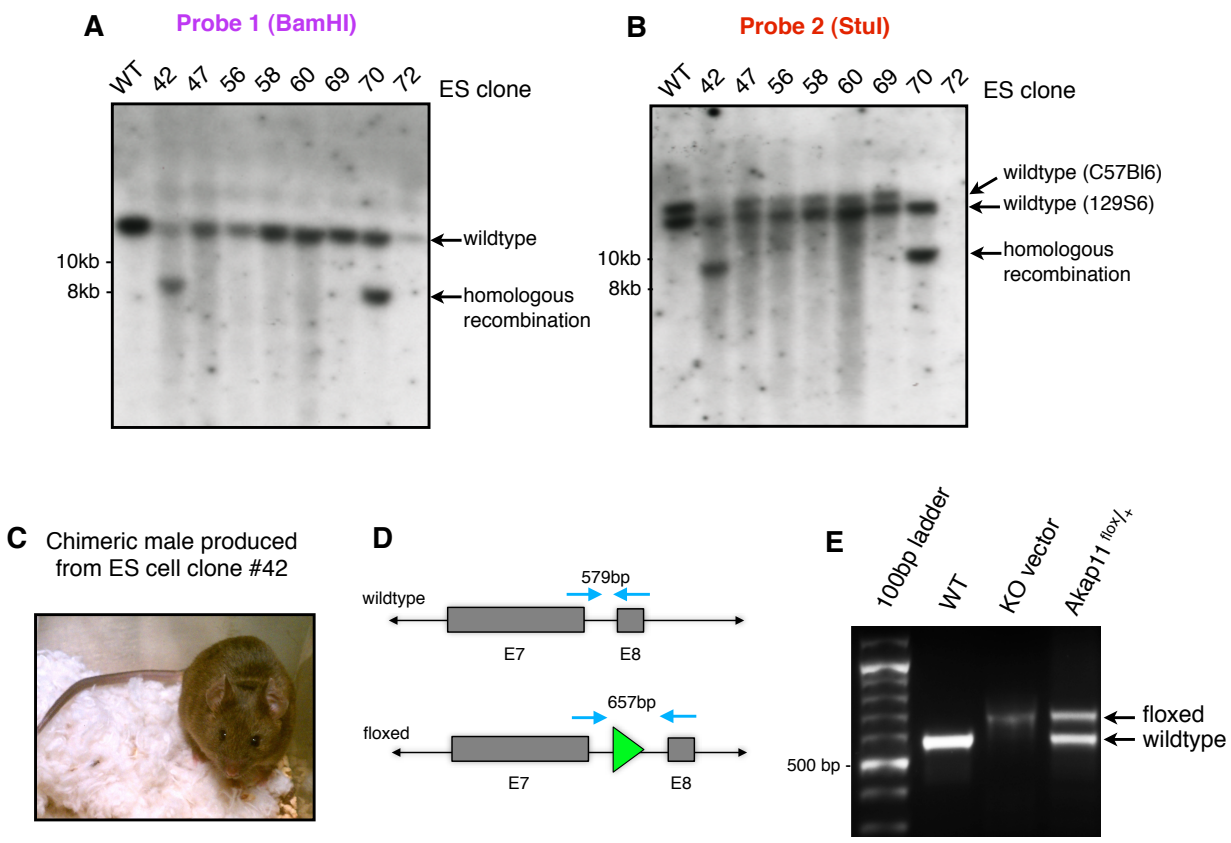

Figure 3.2: Southern blot selection of ES clones for production of the *Akap11* conditional knockout mouse. A) Genomic DNA was harvested from ES clones, digested with BamHI and hybridized with a radiolabeled DNA-probe complementary to a region between *Akap11* Exons 2 and 3. The expected band size for the wild-type and recombined alleles were 13.0kb and 8.3kb, respectively. The recombined band was detected in both clones #42 and #70, confirming homologous recombination of the 5' arm. B) Genomic DNA harvested from the same clones was digested with StuI and hybridized with a radiolabeled DNA-probe complementary to a region between *Akap11* Exons 8 and 9. The expected band sizes for the C57Bl/6J wild-type and recombined alleles were 18.4kb and 9.3kb, respectively. The apparently S129S wild-type band is detected at ~17kb. Homologous recombination of the 3' arm was confirmed for ES clones #42 and #70, confirming that these clones successfully incorporated the knockout vector at the appropriate genetic locus. C) Three chimeric offspring resulted from blastocyst injection and implantation of these clones. Pictured here is a 99% agouti chimeric male produced from clone #42. D) Genotyping primers represented by blue arrows were designed flanking the 3' loxP site to allow identification of the wild-type or floxed allele. E) The chimeric male generated from Clone #42 was crossed to a wild-type C57Bl/6J female and germline transmission of the floxed *Akap11* allele was confirmed by PCR analysis. Wild-type DNA and the purified knockout vector served as control templates to confirm expected band sizes with the primer pair used in this genotyping reaction.

Breeding to EIIa-Cre

To delete the Neo cassette from the genome, male floxed animals were bred to female mice expressing Flp recombinase (B6(C3)-Tg(Pgk1-FLPo)10Sykr/J). Offspring were tested for the FLP and Neo genes by PCR. The floxed, Neo-negative animals were backcrossed again onto C57Bl/6J. Once this was complete, homozygous *Akap11* lox/lox females were bred to male EIIa-Cre mice for global deletion (Fig. 3.3A). The *cre* transgene is actively transcribed prior to implantation in the uterine wall, resulting in global deletion of floxed genes in all cells of the embryo. Offspring from the initial cross were generally mosaic, with incomplete deletion of the *Akap11* gene. Therefore the mosaic mice were backcrossed to C57Bl/6J to allow germline transmission of the collapsed *Akap11* allele, producing true heterozygous animals (*Akap11*$^{-/+}$) (Fig. 3.3B). The mouse colony was then backcrossed onto a C57Bl/6J genetic background for more than seven generations. Production of true knockout animals was confirmed by PCR genotyping and western blot analysis of tissue extracts (Fig. 3.3C).

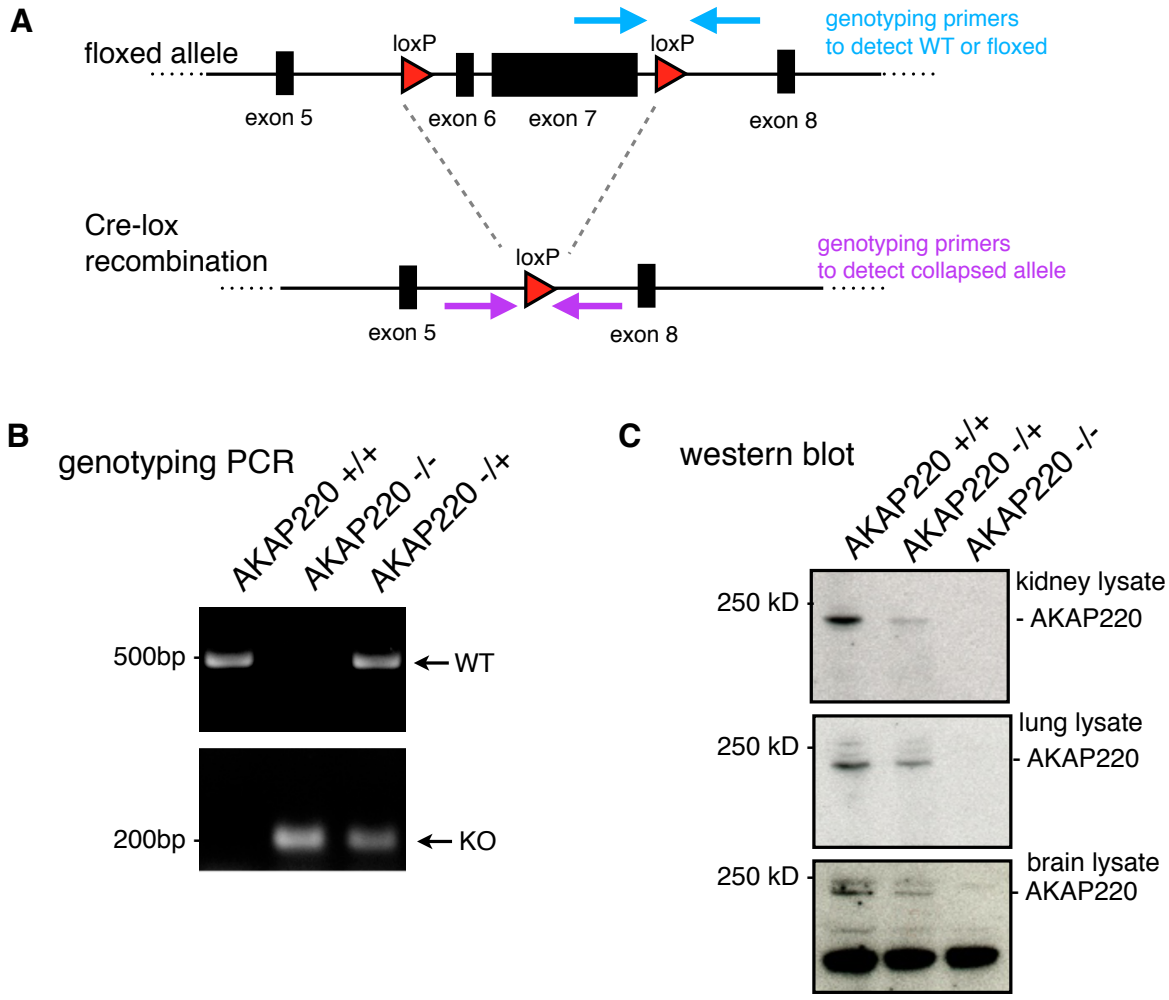

Figure 3.3: Global knockout strategy and confirmation. A) Schematic representation of the additional primer pair designed to detect loxP collapse and deletion of the *Akap11* gene. Two PCR reactions allow for differentiation of wild-type, floxed, or knockout alleles. B) Example PCR products from these reactions demonstrate successful deletion of loxP sites in animals expressing the EIIa-Cre transgene. C) Western blot analysis of kidney, lung, and brain tissue lysates from wild-type, AKAP220$^{-/+}$ and AKAP220$^{-/-}$ mice.

Chapter 4

Phenotypic analysis of AKAP220 global knockout mice

Introduction

Water homeostasis is tightly regulated to maintain blood volume, electrolyte balance, and plasma osmolality. Aquaporin (AQP) proteins are a family of water channels that play an integral role in this process by facilitating passive water transport across the plasma membrane in response to osmotic gradients [53]. These proteins assemble into tetramers, with each monomer possessing a water-permeable pore [54]. To date, thirteen aquaporins have been identified in humans, of which at least seven are expressed in the kidney [55]. Within this family, only aquaporin-2 (AQP2) is known to change subcellular localization in response to hormone regulation, however the molecular pathways that govern AQP2 trafficking remain largely unknown. My research has focused on elucidating the role of AKAP220 signaling complexes in this process.

The kidney nephron

Regulation of water homeostasis primarily occurs in the kidneys, the principal organ of the urinary system. The kidney has evolved to regulate electrolyte and water levels, maintain blood volume and pH, and eliminate metabolic waste products through the production of urine. In a typical, healthy adult the kidneys will filter approximately 180L of blood each day [56]. Most of this is reabsorbed, leading to a net production of 1-2L daily urine output in healthy adults [56].

The functional unit of the vertebrate kidney is the nephron, a highly specialized structure that utilizes both passive and active transport of water and solutes [57]. The average number of nephrons is ~1 million per kidney, but this number can vary by individual anywhere from 200,000 to 2.5 million [57]. The tubular nephron begins at the Bowman's capsule, a cup-shaped sack surrounding a capillary bundle known as a glomerulus. As blood passes through the capillary bed, hydrostatic forces allow water, ions, and small solutes to pass into the tubular blood filtrate while large proteins and platelets remain in the blood [58].

The blood filtrate is isoosmotic with the surrounding interstitium as it enters the next segment of the nephron, the proximal convoluted tubule. Here, more solutes are secreted into the filtrate including creatine, uric acid, and antibiotics [59]. In addition, solutes such as sodium, potassium, glucose, amino acids and bicarbonate are actively and passively reabsorbed back into the bloodstream. This segment expresses AQP1 and allows water reabsorption into the mildly hyperosmotic interstitium [60,61].

Next, the filtrate passes into the loop of Henle. This is a hairpin-shaped stretch of tubule that dips into the kidney medulla. The descending limb of the loop expresses AQP1 and is permeable to water but not solutes [60,61]. Water leaves the tubule, causing the filtrate to become more concentrated as it progresses into the thick ascending limb. This region does not express aquaporins and is therefore relatively impermeable to water [62]. However, solutes such as sodium and calcium are actively reabsorbed to generate a hyperosmotic medulla [62]. As these solutes are pumped into the interstitium, water reabsorption increases from the nearby descending limb in a positive feedback loop. This mechanism is known as countercurrent exchange, and it is responsible for generating the hypertonic interstitium required to facilitate passive water reabsorption from the tubule [63].

The final segment of the nephron is the collecting duct, a region of regulated water reabsorption. In collecting duct cells, AQP3 and AQP4 are constitutively expressed on the basolateral (blood-facing) membrane[64]. Localization of AQP2, however, is regulated by arginine vasopressin (AVP), also known as antidiuretic hormone (ADH)[65]. It is released from the posterior pituitary in response to dehydration. Under resting

conditions, AQP2 is stored on intracellular vesicles in the principal cells of the collecting duct [66]. Vasopressin signaling activates the Gs-coupled vasopressin receptor (V2R), stimulating a cAMP-mediated cascade and causing AQP2-containing vesicles to fuse with the apical (lumen-facing) membrane[67]. Water passes out of the collecting duct, resulting in excretion a concentrated, less dilute urine.

Closely surrounding the nephron is the vasa recta, a capillary bed after the glomerulus that lies parallel to the loop of Henle [68]. The blood in the vasa recta flows in the opposite direction of the blood filtrate, allowing solutes and water reabsorbed into the medullary interstitium to re-enter the circulatory system [68]. These capillaries also contribute to secretion of ions, glucose, and metabolites that can enter the tubule through passive or active transport.

The evolution of the nephron represents an important evolutionary step for survival of land-dwelling mammals. Renal failure, drug toxicity, injury or genetic mutation can impair water or solute transport. Diseases causing defective water conservation can lead to osmotic shock, electrolyte imbalance, and life-threatening dehydration.

Diabetes Insipidus

Diabetes insipidus is a disease characterized by excessive thirst (polydipsia), excessive urination (polyuria), high blood sodium (hypernatremia) and dehydration[69]. There are two main classes of diabetes insipidus: central (CDI) and nephrogenic (NDI) [70]. Both forms of diabetes insipidus result in defective water reabsorption, yet the causes and severity vary greatly [69,71]. Infants born with congenital forms are at risk of complications if the disease is not diagnosed early. Repeated bouts of severe dehydration can cause delayed development and mental retardation [72].

Central diabetes insipidus (CDI) is caused by loss of vasopressin production or release from the hypothalamus or posterior pituitary gland [73]. CDI can be acquired through damage to the hypothalamus or pituitary by injury, tumor, surgery, or infection[74]. Some cases are idiopathic, with no known cause, and may be temporary[75]. Inherited forms of CDI are rare and typically caused by autosomal dominant mutations in the vasopressin gene[76,77]. Mild CDI cases are managed with low sodium diet and increased water intake.

More severe cases are often treated with desmopressin (DDAVP), a synthetic vasopressin analogue that can be administered nasally, orally, or intravenously[69].

Nephrogenic diabetes insipidus (NDI) is more rare. It can be caused by autosomal dominant mutations in AQP2 that prevent normal expression or trafficking of the channel. Most known mutations cause the channel to be retained in the endoplasmic reticulum, likely due to misfolding or translation stalls [71]. However, NDI is most commonly caused by X-linked mutations in the vasopressin receptor (V2R) that prevent folding, activation or coupling to Gs [76]. Because of this, desmopressin treatment is ineffective in NDI. In fact, circulating levels of endogenous vasopressin are often elevated in NDI due to lack of feedback inhibition [78].

Paradoxically, thiazide diuretics can relieve symptoms of NDI [79]. These drugs inhibit sodium reuptake in the distal convoluted tubule, increasing both sodium and water levels inside the tubule. This decreases extracellular volume and slows the glomerular filtration rate, causing the blood filtrate to progress through the tubule more slowly [79]. The mechanism is not completely understood, but it is believed that by slowing the blood filtrate allows more time for water reabsorption through AQP1 in the descending limb, reducing the amount of water delivered to the collecting duct and lost as urine [79].

Apart from low-sodium diet and increased water intake, diuretics remain the only pharmacological treatment for NDI, but they have limited efficacy and potential negative side effects. Therefore, a medical need exists for new therapeutic avenues to treat NDI. Because 90% of congenital NDI causes are caused by mutations in the vasopressin receptor, activating the AQP2 signaling pathway downstream of the receptor is an attractive drug target. However, the mechanisms governing AQP2 shuttling to the plasma membrane are not understood. Therefore, understanding this signal transduction pathway is of clinical significance.

AQP2 phosphorylation and trafficking

AQP2 is the only water channel known change its subcellular distribution in response to signaling events. The molecular details of this signaling pathway are largely unknown, but phosphorylation plays an integral part of the process. There are four conserved

serine residues on AQP2 regulated in response to vasopressin stimulation: S256, S261, S264, S269 [80-83]. PKA-dependent phosphorylation of S256 is perhaps the best studied, and is known to play an important role in triggering exocytosis of AQP2 containing vesicles [33]. This site is a target for protein kinase A, Golgi casein kinase, protein kinase G. Of these, PKA has the largest known role in stimulating fusion of AQP2-containing vesicles with the apical membrane following activation of the vasopressin Gs-coupled receptor. Many studies have confirmed that cAMP-elevating agents including desmopressin, forskolin, and dibutyryl cAMP all stimulate increased pS526 and relocalization to the plasma membrane.

Mutational analysis of S256 has demonstrated that a non-phosphorylatable mutant (S256A) is retained in intracellular vesicles while a phosphomimetic mutant (S256D) is constitutively expressed at the apical membrane [66,84]. Interestingly, evidence suggests that phosphorylation of S256 is a pre-requisite for phosphorylation of S264 and S269 (but has no effect on phosphorylation of S261) [85]. Although pS256 is necessary and sufficient for AQP2 translocation, the maintenance of membrane localization likely involves additional regulatory events. For example, PKA inhibition with H-89 causes internalization of AQP2-S256D, suggesting this kinase may act upstream of additional AQP2-regulating molecules to maintain localization of the channel at the apical membrane [86].

Phosphorylation of S269 also increases in response to vasopressin, and there is evidence to suggest this site regulates AQP2 internalization from the plasma membrane [85]. S269A mutants have normal redistribution to the plasma membrane in response to vasopressin, but a phosphomimetic S269D mutant accumulates at the membrane even in the absence of stimulation [87]. This suggests that phosphorylation at S269 likely plays no role in cAMP-mediated exocytosis of AQP2, but may regulate endocytosis.

The roles of S264 and S261 phosphorylation events are less understood. Vasopressin stimulates a 4-fold increase in pS264, but the effects on localization are not clear as pS264-AQP2 has been detected at the apical and basolateral membranes, as well as clathrin-coated vesicles and early endosomal compartments [81]. Interestingly, S261 is highly phosphorylated under basal conditions, 24-fold higher than S256 [67]. It has been

suggested that S261 plays a reciprocal role on AQP2 localization, as pS261 levels drop in response to vasopressin stimulation [83]. More experiments are necessary to determine whether pS261 regulates maintenance of AQP2 on intracellular vesicles in the absence of vasopressin signaling.

One study utilized phosphomutants to study the effects of phosphorylation at each site on AQP2 stability [87]. This work demonstrated that phosphomimetic S256D and S269D forms had reduced internalization rates and increased protein half-lives [87]. These changes correspond with reduced interaction between AQP2 and endocytic proteins Hsp70, Hsc70, dynamin, and clathrin heavy chain [87]. Together these data suggest that AQP2 is stabilized when localized to the plasma membrane, but whether this is caused by active regulation of endocytosis and/or degradation pathways remains to be determined.

It has also been suggested that phosphorylation of aquaporin channels may influence channel gating and water permeability, although conflicting reports exist. One study expressed the S-A or S-D mutant forms of all four vasopressin-regulated phosphosites in *Xenopus* oocytes and found no change in water permeability for any mutant compared to wild-type AQP2 [87]. However, another study using purified AQP2 protein reconstituted into liposomes *in vitro* found increased water permeability in both phosphorylated wild-type AQP2 and the S256D phoshomimetic, perhaps through induced conformational changes [88]. Therefore, future studies are needed to determine whether AQP2 channels are gated and if phosphorylation plays a role in this process.

Phosphatases and AQP2

As differential phosphorylation of AQP2 regulates localization, it is important to consider the influence of both kinases and phosphatases on this pathway. Few studies have been done on this subject, but both PP1 and PP2A activity have been implicated in AQP2 regulation. Treatment with 1 μM okadaic acid is sufficient to induce AQP2 phosphorylation and translocation to the plasma membrane [89]. Phosphorylation analysis with purified proteins suggests Ser256 is primarily a PP2A substrate, while Ser269 is a PP1 substrate [35]. Therefore, PP1 anchored by AKAP220 may influence endo- or

exocytosis of AQP2 channels by regulating the balance of phosphorylation and dephosphorylation of various residues on the cytoplasmic tail of the water channel.

Interestingly, treatment with H89 was able to prevent the increase in AQP2 phosphorylation following okadaic acid treatment, but did not prevent redistribution of the water channel to the apical membrane [89]. This suggests that PKA-dependent phosphorylation is not strictly required for AQP2 translocation, at least under conditions where PP1 or PP2A activity is inhibited. It is possible, then, that PP1 or PP2B could regulate mechanisms required for maintenance of AQP2 in the vesicular compartment under resting conditions. Perhaps that these studies have begun to shed light upon a new branch of AQP2 regulation that is not fully appreciated.

Ubiquitination and internalization of AQP2

The primary focus of AQP2 research has been placed on the exocytic mechanisms that govern its translocation to the plasma membrane. However, the endocytic pathways are equally important for regulating water homeostasis and must also be tightly controlled. Both prostaglandin E2 and dopamine signaling have been shown to induce AQP2 internalization through activation of protein kinase C (PKC) [86,90]. Subsequent analysis discovered that either AVP withdrawal or direct PKC activation causes K63-linked ubiquitination at K270 [91]. This occurs preferentially at the plasma membrane, and surface biotinylation experiments indicate ubiquitination precedes channel internalization [91]. The vesicles are sorted to multivesicular bodies for lysosomal degradation, decreasing the total AQP2 levels.

AQP2 and the actin barrier

Specific signaling events such as PKC activation may occur to initiate internalization of AQP2 when water levels return to normal, however additional cytoskeletal mechanisms exist to maintain this internalized state. The actin cytoskeleton was known to regulate vasopressin-responsive water permeability even before AQP2 was discovered [92]. Original studies of toad urinary bladders demonstrated reversible actin depolymerization following treatment with vasopressin, forskolin, or 8-Bromo-cAMP [93]. Microscopic analysis revealed that the majority of vasopressin-responsive actin depolymerization

occurs at apical pole[94]. This is interesting because the principal cells of the collecting duct have a uniquely thick actin meshwork at the apical membrane that is not observed in collecting duct cells that do not express AQP2, called intercalating cells [95]. In fact, studies using several MDCK and LLC-PK1 cell lines with variable AQP2 expression demonstrated a significant correlation between AQP2 expression level and actin depolymerization in response to vasopressin [96].

Based on this information, it has been proposed that a network of cortical actin serves as a physical barrier preventing basal fusion of AQP2-containing vesicles with the apical plasma membrane. Treating cultured IMCD cells with the actin-depolymerizing drug cytochalasin-D causes translocation of AQP2 even in the absence of vasopressin or cAMP-elevating agents [97]. Inhibition of the Rho family of small GTPases with *C. difficile* toxin B reduces cortical f-actin staining and redistributes AQP2 to the membrane, even in the absence of vasopressin stimulation [97]. To tease apart which Rho-family GTPase was responsible for maintaining the cortical actin barrier, *Clostridium botulinum* C3 toxin was microinjected into cells to specifically inhibit RhoA. This toxin was sufficient to induce AQP2 translocation, and effect that was also mimicked by inhibiting downstream effectors of RhoA with the drug Y-27632 [97]. When a consitutively active RhoA was expressed in CD8 cells, stress fibers formed and AQP2 no longer trafficked to the plasma membrane following forskolin stimulation [98].

Researchers have been able to link vasopressin signaling to reduced RhoA activity through PKA [99]. In response to elevated cAMP, PKA phosphorylates RhoA at Ser188, increasing its association with the Rho GDP dissociation inhibitor (RhoGDI)[100]. Once bound, RhoGDI inhibits RhoA from binding other downstream effectors, regardless of its GTP- or GDP-bound state [100,101]. Therefore, vasopressin stimulation increases PKA phosphorylation of RhoA to inhibit its activity and sequester it away from effector molecules through RhoGDI sequestration [99]. Together, these data strongly support a role for RhoA in the production and/or maintenance of the actin barrier when vasopressin signaling is absent and body water levels are within the normal range.

AKAPs and AQP2

In light of such bi-directional regulatory mechanisms, signaling scaffolds that anchor both kinases and phosphatases become relevant to AQP2 trafficking. In fact, compartmentalized PKA anchored to AKAPs is required for vasopressin-induced translocation to the plasma membrane [102,103]. Treatment of cultured inner medullary collecting duct cells with the PKA anchoring disruptor peptide St-Ht-31 or the PKA inhibitor H89 completely abolished AQP2 translocation in response to AVP or forskolin [103]. It is likely that AQP2 associates with multiple different AKAP signaling complexes as it cycles through the exocytic and endocytic compartments. These AKAPs may supply a changing compliment of kinases, phosphatases and phosphodiesterases to regulate the phosphorylation of AQP2 as it traffics through the cell. Microarray analysis of cultured rat IMCD cells detected expression of ten known AKAP genes, and the highest expressed were AKAP-7, -8, 9, -11, and -13 [104]. Interestingly, the AKAP11 signal was an order of magnitude higher than any other AKAP, potentially highlighting the importance of AKAP220 in IMCD cells. How these expression patterns translate to protein abundance remains to be tested.

One experiment attempted to identify which AKAPs are associated with AQP2-containing vesicles with a far western blot assay using purified PKA regulatory subunit. This method detected several AKAP bands in the particulate cell fraction of IMCD cells [105]. This led to future studies identifying a novel splice variant of AKAP18 (AKAP18δ) associated with IMCD vesicles [106]. An antibody was produced for AKAP18δ was used to isolate intracellular vesicles for western blot analysis. AQP2 protein was enriched in the AKAP18δ vesicle pulldowns compared to controls, and this increase was observed for both glycosylated and non-glycosylated forms[106]. This work was unable to demonstrate a direct interaction between AKAP18δ and AQP2, suggesting the two proteins co-localize on a distinct pool of intracellular vesicles but may not physically bind to each other.

Interestingly, global deletion of all four AKAP18 isoforms (AKAP18α, β, γ, and δ) has no overt effect on water reabsorption or urine production. Although rigorous studies are still needed, the global AKAP18 knockout mice have no symptoms to suggest a diabetes insipidus phenotype (unpublished data, McKnight lab, University of Washington). Because vasopressin-responsive translocation of AQP2 containing

vesicles requires an anchored pool of PKA, additional AKAPs are likely involved. However, although several RII-binding bands were detected in the particular fraction of IMCD cells, the only other AKAP that has been identified as an AQP2 interacting partner is AKAP220.

AKAP220 and AQP2

AKAP220 was first identified as an AQP2 interacting partner by yeast two-hybrid screen[27]. Immunohistochemistry and immunogold labeling of rat kidney sections detected co-distribution in collecting ducts, with the signals primarily localized in the cytosolic compartment. Mutational analysis mapped the binding interface between AKAP220 residues 1085-1174 and the cytoplasmic carboxy tail of AQP2 [27]. This region of AQP2 contains the previously discussed vasopressin-regulated phosphosites (S256, S261, S264, S269), suggesting AKAP220 may anchor important regulatory kinases and phosphatases with the water channel. In fact, co-expression of AKAP220 with AQP2 in COS cells enhances the phosphorylation of AQP2-S256 in response to forskolin treatment [27].

Several AKAP220 binding partners are known to regulate AQP2 phosphorylation or localization, including PKA, GSK3β, and PP1 [34,35,84]. Conditional knockout mice lacking GSK3β specifically in renal collecting ducts have decreased AQP2 mRNA expression and reduced AQP2 protein abundance, phosphorylation and localization to the apical membrane [34]. Interestingly, conditional GSK3β knockout mice also have reduced adenylyl cyclase activity, an effect mimicked by pharmacological inhibition of GSK3β. Therefore, it is believed that GSK3β activity supports cAMP production in response to vasopressin.

In addition to simply anchoring enzymes that influence AQP2 regulation, AKAP220 has also been shown to regulate cytoskeletal dynamics and cortical actin polymerization [25,26]. Our lab has shown that siRNA-mediated knockdown of AKAP220 reduces cortical f-actin staining and membrane ruffle formation [25]. Therefore, AKAP220 signaling complexes may regulate actin barrier production, maintenance, or reorganization in the principal cells of the collecting duct. The work described here begins to examine this

hypothesis, though many experiments are still needed to elucidate the causes and implications of the findings described here.

Understanding the mechanisms that govern AQP2 regulation is of clinical relevance for the treatment of water handling disorders such as nephrogenic diabetes insipidus. Growing evidence supports a functional role for the macromolecular complex including AKAP220, AQP2, PKA, GSK3β, PP1, and the actin cytoskeleton in this process. We therefore became interested in studying water reabsorption in the AKAP220$^{-/-}$ mouse model. In these studies we discover that global AKAP220 knockout animals do not dilute urine appropriately in response to acute water loading. This effect is likely caused by the redistribution of AQP2 to the apical membrane of the collecting ducts in these mice, even when they are over hydrated. Interestingly, RhoA is also restricted to the apical membrane, and evidence suggests the level of GTP-bound, active RhoA is reduced in kidneys from knockout mice compared to wild-type. Together, these data support a role for AKAP220 in maintaining AQP2 in vesicles in the absence of vasopressin-mediated signaling, potentially through the maintenance of the cortical actin barrier.

RESULTS:

AKAP220$^{-/-}$ mice have reduced body size – Global deletion of AKAP220 did not cause embryonic lethality, and we observe no reproductive deficits in knockout animals. Heterozygous (AKAP220$^{-/+}$ x AKAP220$^{-/+}$) and homozygous (AKAP220$^{-/-}$ x AKAP220$^{-/}$) crosses readily produce pups with expected Medelian ratios, and knockout crosses are also able to breed successfully without issue. AKAP220$^{-/-}$ mice have normal appearance, mobility, and lifespan. The only overt phenotype was a reduced body size, as knockout pups were often runted compared to wild-type littermates and had reduced total body weight (Fig. 4.1).

We hypothesized the change in body weight was due to overall reduced body size rather than leanness, as body length measured from the tip of the snout to the base of the tail was also reduced (Fig. 4.1C). Using metabolic cages we tested whether food

and water intake were normal compared to wild-type mice. The bottom of the metabolic cages funneled urine and fecal matter into collection basins. Mice were allowed to acclimate to the cages for four days. Total body weight, feces, urine, food and water measurements were recorded every 24 hours for 3 days.

The raw measurements of intake and output were all reduced for the AKAP220$^{-/-}$ mice compared to wild-type (Fig. 4.1C). However, AKAP220$^{-/-}$ animals have reduced body size, so these values were normalized to total body weight (%BW) to determine if the reductions were proportionate to size. Once normalized, no significant changes were seen in water intake, food intake, urine production or fecal output (Fig. 4.1 A-B). Together these results suggest the AKAP220$^{-/-}$ mice have a dwarf phenotype not caused by altered food intake or leanness. This important discovery also clearly proves that AKAP220$^{-/-}$ animals do not suffer from diabetes insipidus, as both water consumption and urine volume were normal.

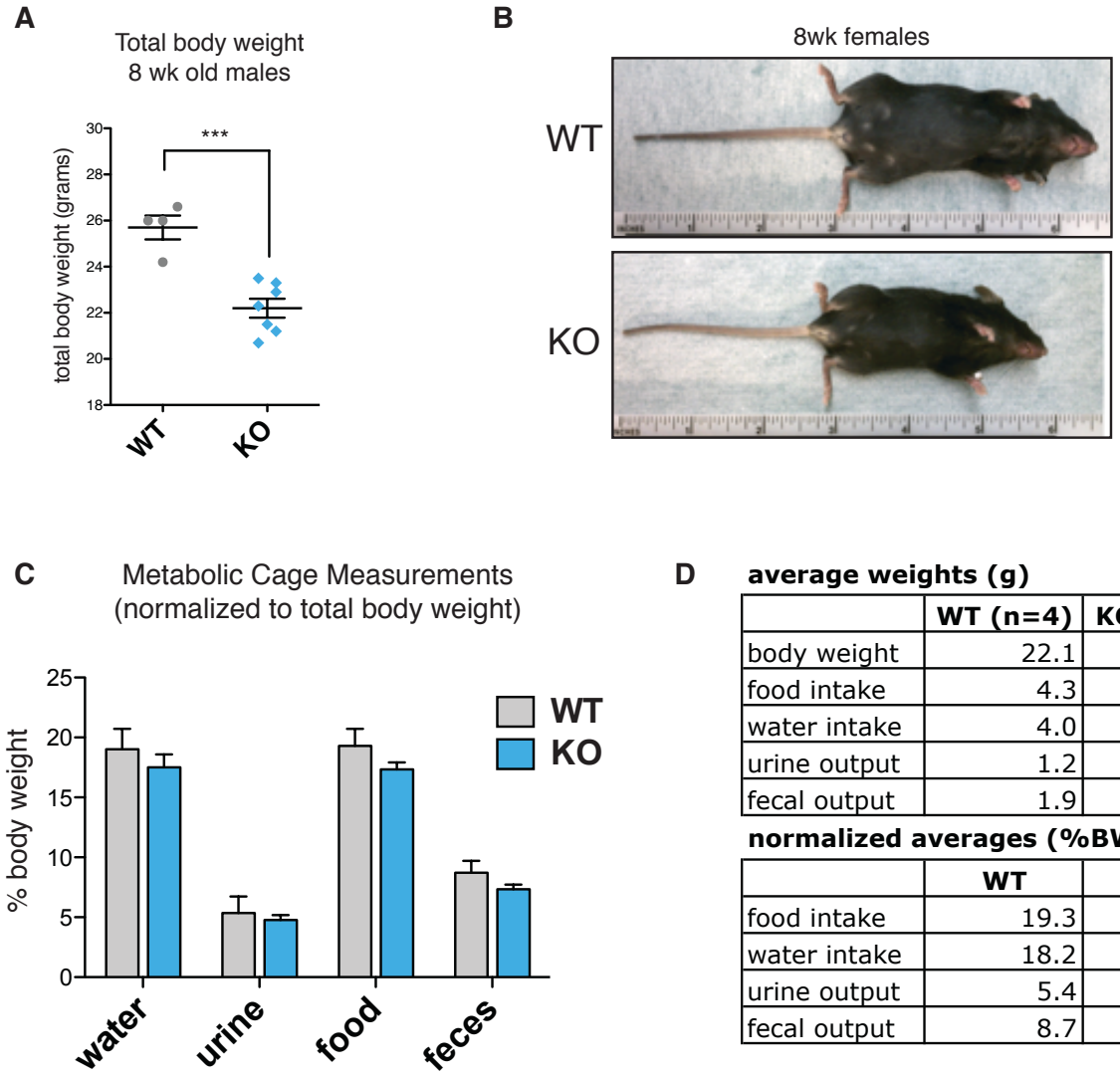

D

average weights (g)

	WT (n=4)	KO (n=4)
body weight	22.1	18.9
food intake	4.3	3.3
water intake	4.0	3.2
urine output	1.2	0.9
fecal output	1.9	1.4

normalized averages (%BW)

	WT	KO
food intake	19.3	17.3
water intake	18.2	16.9
urine output	5.4	4.8
fecal output	8.7	7.3

Figure 4.1: AKAP220$^{-/-}$ mice have reduced body size. A) Adult male mice were weighed at 8wks of age. Knockout mice have a statistically significant reduction in total body weight. B) Respresentative images of 8wk old female mice. Knockout mice have reduced body length. C) Food and water intake were measured for wild-type and knockout mice, and both urine and fecal outputs were recorded. No significant differences were observed between groups in any of the measured parameters. D) Average raw values (grams) for both groups were normalized to total body weight to account for reduced body size in AKAP220$^{-/-}$ mice.

AKAP220$^{-/-}$ mice have reduced urine-diluting capacity

Although the AKAP220$^{-/-}$ mice did not show symptoms of diabetes insipidus, we hypothesized that AKAP220 may anchor AQP2 with signaling enzymes to regulate the function, localization, and/or trafficking of the water channel. Therefore we decided to measure urine concentration (osmolality) as a simple test of water reabsorption capacity. Urine samples were collected from animals that were either given free water access (*ad libidum*), dehydrated for 24hr (complete water restriction), or subjected to acute water loading by oral gavage (3% total body weight). The concentration of urine samples from each group was measured using a vapor pressure osmometer.

We found no difference in urine osmolality between wild-type and AKAP220$^{-/-}$ mice given *ad libitum* access to water (Fig. 4.2A). The average urine osmolality in wild-type animals was 1033 mmol/kg, compared to 939 mmol/kg in AKAP220$^{-/-}$ mice. Likewise, both groups produced concentrated urine following 24 hours of dehydration. Average dehydrated urine concentration for wild-type was 2832 mmol/kg, and 2628 mmol /kg for knockout animals (Fig. 4.2B). These data confirm that the vasopressin system is intact in the knockout mice, as these animals readily responded to dehydration by producing concentrated urine.

To test the effects of overhydration, animals were administered a 10% glucose solution by oral gavage equal to 3% of their total body weight. This dosage has been shown previously to cause a rapid drop in urine osmolality (~300 mmol/kg, [107]). Under these conditions, urine osmolality decreased compared to baseline in both groups, however urine osmolality was significantly higher in knockout animals (460.1 mmol/kg) compared to wild-type controls (262.4 mmol/kg) (Fig. 4.2C). This result indicates defective urine diluting capacity in response to acute over-hydration, causing the animals to exhibit mild water retention and produce more concentrated urine than wild-type controls.

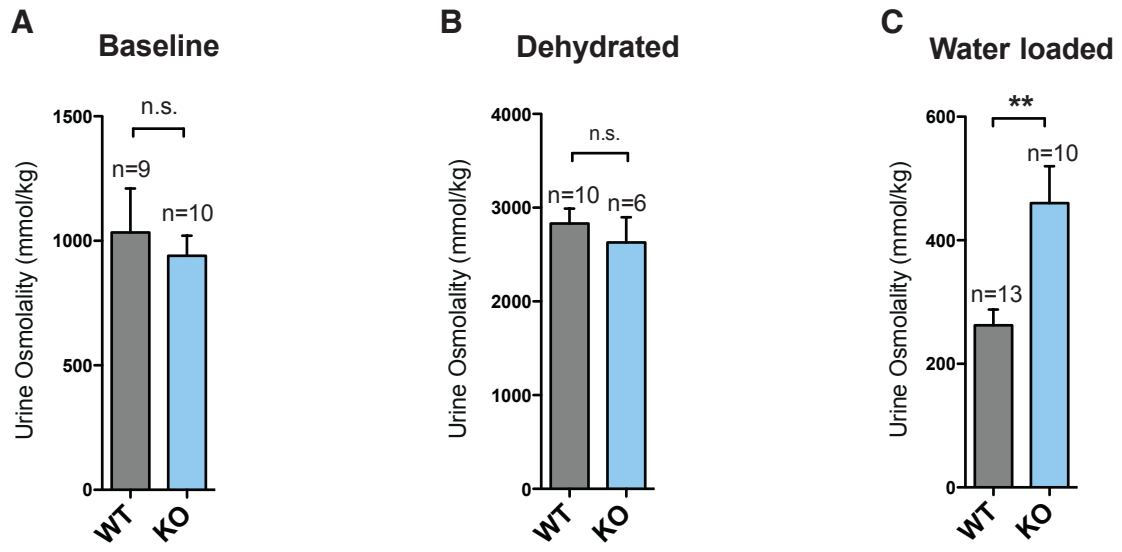

Figure 4.2: AKAP220 knockout animals are unable to dilute urine properly in response to acute water loading. Urine samples were collected from wild-type and AKAP220$^{-/-}$ animals that were given *ad libitum* water access, complete water restriction, or acute water loading A) The baseline group was given *ad libitum* water access for 24hr prior to sample collection. Urine osmolality was unchanged between wild-type and knockout animals. B) Dehydrated animals had complete water restriction for 20 hours prior to the experiment. Again, no difference was detected between wild-type and knockout animals. The increase in urine osmolality compared to baseline indicates that the vasopressin system is intact in AKAP220 knockout mice. C) The water-loaded group was given an oral gavage equal to 3% total body weight 30min prior to urine collection. Urine osmolality decreased compared to baseline for both wild-type and knockout. However, knockout animals produced significantly more concentrated urine than wild-type, suggesting inappropriate water reabsorption even during periods of overhydration.

AKAP220$^{-/-}$ mice have increased AQP2 expression – Based on the decreased excretion of water during over-hydration, we hypothesized that AQP2 expression or localization may be altered in AKAP220$^{-/-}$ mice. Because the channel allows passive water transport across an osmotic gradient, over-expression, stabilization or mislocalization at the apical plasma membrane could cause the observed phenotype.

To test this hypothesis we isolated kidneys from wild-type and AKAP220$^{-/-}$ mice. The medulla was dissected from the cortex, and tissue extracts were generated for western blot analysis. AKAP220 was detected in both the medulla and cortex of wild-type kidneys and was completely absent in knockout tissue (Fig. 4.3A). As expected, AQP2 was not detected in kidney cortex in either wild-type or knockout samples, confirming the specificity of the antibody used. Interestingly, both the glycosylated and non-

glycosylated forms of AQP2 protein were increased in AKAP220 knockout compared to wild-type (Fig. 4.3A). A similar increase was seen for phospho-Ser256 AQP2 (Fig. 4.3A). Whether this is a true increase in phospho-Ser256 or an apparently increased caused by higher levels of total AQP2 remains unclear from this experiment.

We next wanted to know if the increase in total AQP2 was caused by mRNA over-expression, protein stabilization or reduced protein degradation. To test AQP2 mRNA expression, kidneys were harvested from animals given *ad libitum* water access and from over-hydrated animals one hour after water loading. Medulla tissue was isolated and prepared for mRNA extraction. The samples were reverse transcribed into cDNA for qPCR analysis using probes for AQP2 and GAPDH. Although a slight upward trend in AQP2 expression was detected in AKAP220$^{-/-}$ tissue from both the baseline and water loaded groups, the difference was not statistically significant (Fig. 4.3B). Therefore, it is unlikely that the observed change in protein level was due to AQP2 over-expression.

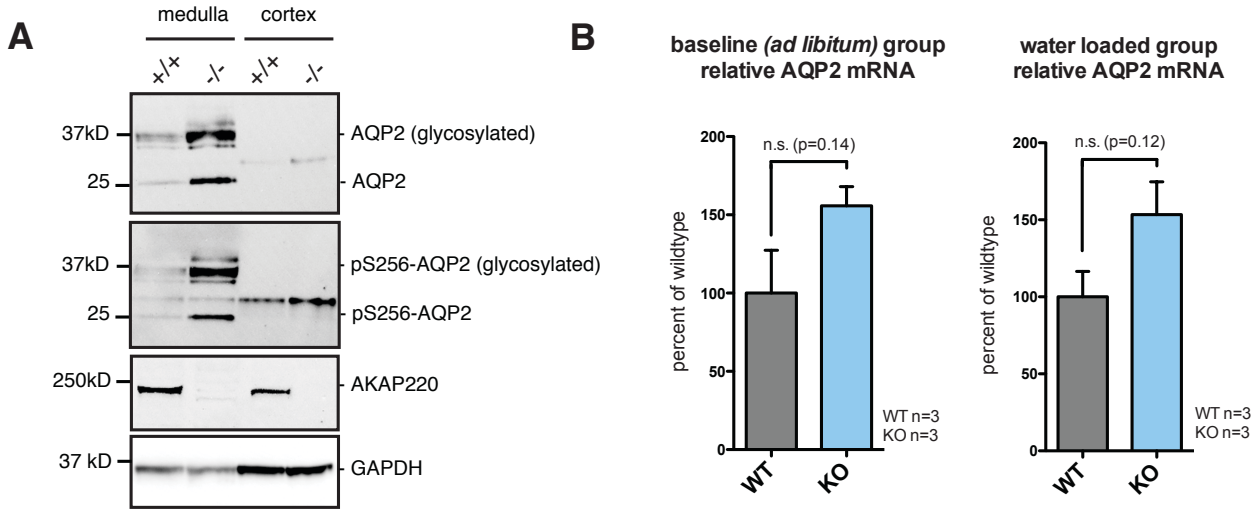

Figure 4.3: AQP2 protein levels are increased in AKAP220$^{-/-}$ kidneys. A) Western blots on tissue extracts from kidney medulla or cortex. Total AQP2 and phospho-Ser256-AQP2 are increased in AKAP220 knockout tissue. Equal loading was confirmed by GAPDH. As expected, no AQP2 was detected in cortex, confirming the specificity of the antibody used. B) Quantitative PCR analysis found no significant difference in mRNA expression of AQP2 in animals that were given *ad libitum* water access or animals that were water loaded (3% total body weight by oral gavage).

We next wanted to test whether the protein increase might be caused by stabilization of the protein. Previous work has shown that AQP2 phospho-mutants with increased membrane localization (AQP2-S256D and S269D) have longer protein half-lives and reduced association with endocytic machinery [85]. This suggests that AQP2 is stabilized in the plasma membrane environment. Therefore, we used immunohistochemistry of kidneys harvested from *ad libitum* and water-loaded animals to test AQP2 localization. The kidneys were immunostained with anti-AQP2 antibodies and imaged by scanning confocal microscopy.

In wild-type tissue, AQP2 had cytosolic, perinuclear and apical membrane localization in the principal cells of the collecting duct (Fig. 4.4A-B). This staining pattern is consistent with AQP2 being endocytosed into vesicles in response to overhydration. In AKAP220$^{-/-}$ kidneys, however, AQP2 signal was more constrained at the apical membrane, adjacent to the lumen of the collecting duct (Fig. 4.4A-B). This is confirmed by line plot analysis of AQP2 fluorescence intensity across the apical membrane of the principal cells (Fig. 4.4C). This observation suggests that the urine phenotype may be due to inappropriate water reabsorption in the collecting duct, as passive water transport could continue even under over-hydrated conditions through AQP2 channels present on the apical membrane.

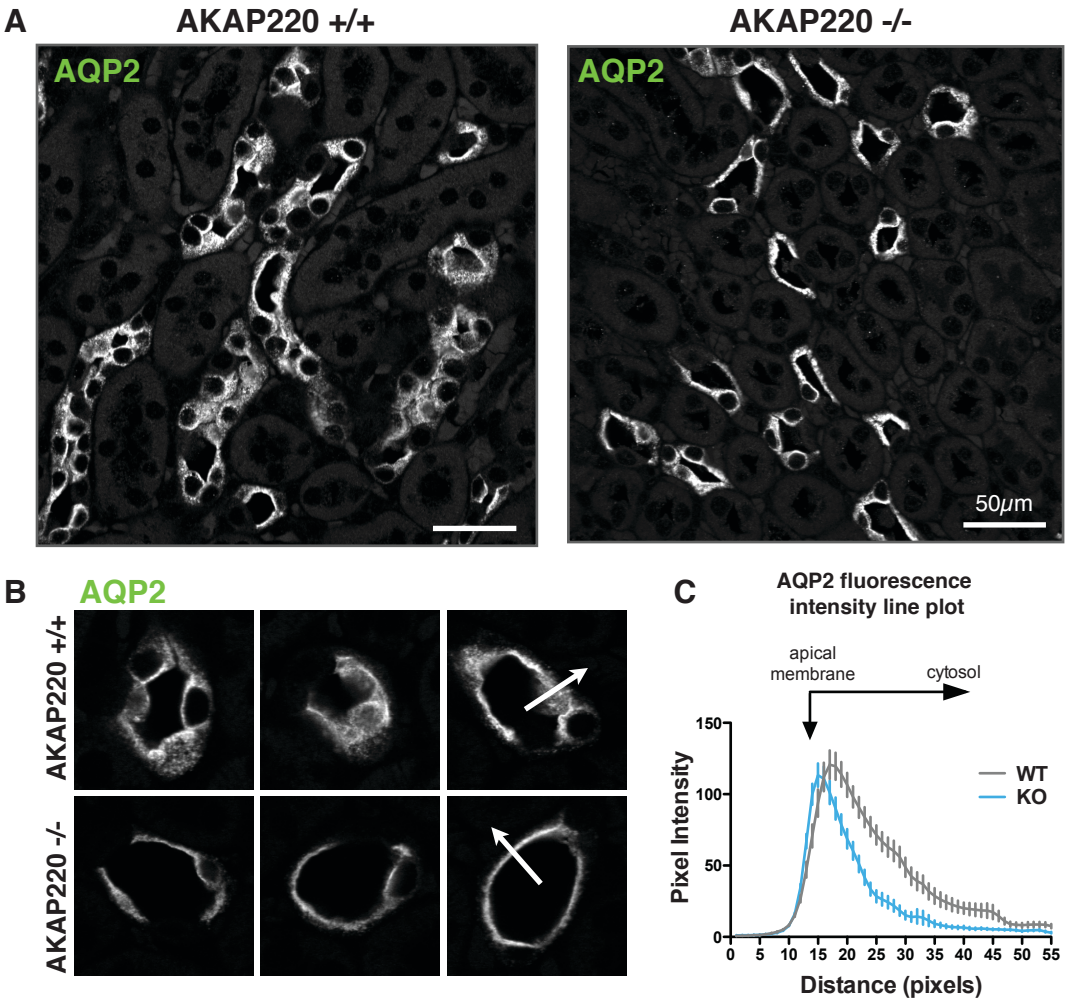

Figure 4.4: AQP2 is restricted to the apical membrane of kidney collecting ducts in AKAP220$^{-/-}$ kidneys. Paraffin embedded kidney sections were obtained from 15-week-old mice, water-loaded with 3% total body weight by oral gavage. A) In wild-type kidneys, AQP2 is detected at cytosolic, perinuclear, and apical membrane locations. B) In AKAP220$^{-/-}$ kidneys, AQP2 signal is more restricted to the apical membrane, with less cytosolic and perinuclear staining. Images obtained by scanning laser confocal microscopy, 40X magnification. Scale bars 50μm. C) Zoomed images of collecting ducts highlight restricted AQP2 localization at the apical membrane in AKAP220$^{-/-}$ kidneys compared to wild-type. Asterisks indicate collecting duct lumens. D) Line plot analysis of AQP2 fluorescence intensity. Pixel intensity was plotted on lines drawn from within the collecting duct lumen perpendicular to the apical membrane (indicated by arrows). AQP2 signal in wild-type cells was distributed throughout the cytosol (gray) but restricted close to the apical membrane in AKAP220$^{-/-}$ kidney (blue).

AKAP220 regulates cytoskeletal dynamics through an interaction with IQGAPs, and localizes signaling elements such as GSK3β to the cortical actin network. In the principal cells of the collecting duct, the apical membrane has a dense network of cortical actin that depolymerizes in response to vasopressin signaling. This actin “barrier” is thought to physically prevent AQP2-containing vesicles from fusing with the membrane under hydrated conditions. Based on this information, we wanted to know whether the restricted localization of AQP2 in AKAP220$^{-/-}$ mice might be caused by defective production of an actin barrier.

Because previous studies have linked activity of the small GTPase RhoA to formation of the actin barrier, we decided to check the localization of this protein in water-loaded mice. Interestingly, we discovered that RhoA and AQP2 had dramatic co-distribution in the principal cells of the collecting ducts. In wild-type tissue, RhoA was present at the apical membrane and throughout the cytosol (Fig. 4.5 A). In AKAP220$^{-/-}$ kidneys, RhoA was enriched at the apical membrane, in a similar pattern to the AQP2 signal (Fig. 4.5A). Line plot analysis of these images demonstrates the redistribution of RhoA to the apical membrane in AKAP220 knockout tissue (Fig. 4.5 B). Although RhoA has never been detected in the AKAP220 signaling complex, it is possible this signaling scaffold interacts with an upstream regulator of RhoA and indirectly controls the subcellular localization of this protein.

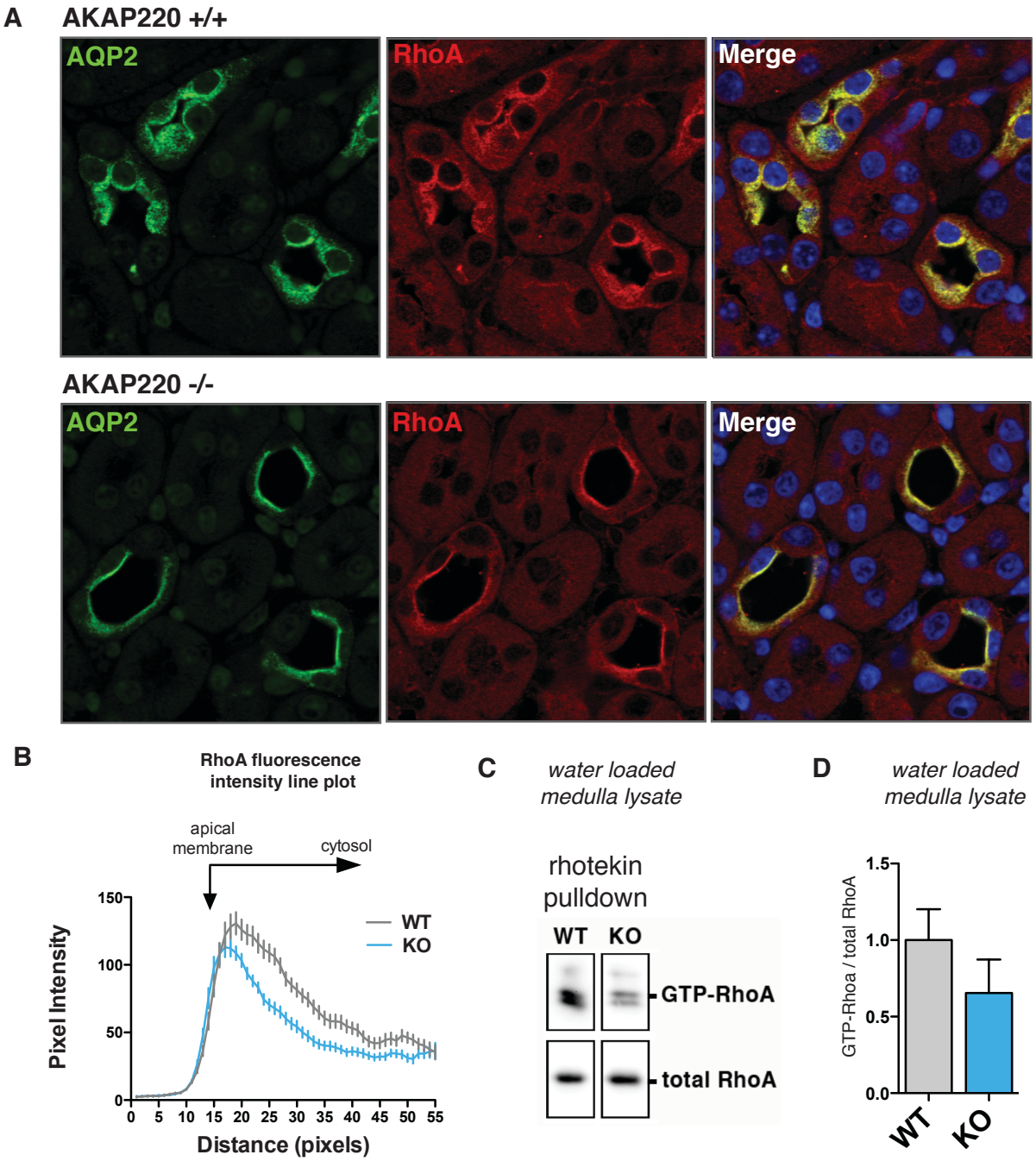

Figure 4.5: RhoA localization and activity is altered in AKAP220$^{-/-}$ kidneys. A) Kidneys were harvested from 15-week-old wild-type and AKAP220$^{-/-}$ mice two hours after acute water loading (3% total body weight by oral gavage). Sections were stained with antibodies against AQP2 (green) and RhoA (red) and DAPI (blue). AQP2 and RhoA co-localized in the principal cells of the collecting ducts. In AKAP220$^{-/-}$ tissue, both AQP2 and RhoA were restricted to the apical membrane of collecting duct principal cells. B) Quantification of RhoA distribution by line plot analysis of fluorescence intensity. C) Medulla lysates from AKAP220$^{-/-}$ kidneys had decreased levels of active, GTP-bound RhoA as detected by Rhotekin pulldown assay. D) Quantification of GTP-RhoA to total RhoA signal intensity, n=3 pulldown experiments.

Additionally, it is possible that AKAP220 signaling complexes are upstream regulators of RhoA activation pathways. To test whether RhoA activity was changed in AKAP220$^{-/-}$ tissue, we performed a pulldown assay that utilizes the Rho-binding domain of the RhoA effector protein, Rhotekin. Tissue extracts were made from wild-type and AKAP220$^{-/-}$ kidney medulla and combined with Rhotekin-agarose beads to isolate only active, GTP-bound RhoA. The ratio of GTP-RhoA signal to total-RhoA input was compared between the two groups. Interestingly, the ratio of active, GTP-bound RhoA was reduced in AKAP220$^{-/-}$ tissue (Fig. 4.5C-D). This data is consistent with the mislocalization of AQP2 being caused by defective actin barrier production, although phalloidin staining for f-actin did not work in the paraffin embedded sections.

Loss of AKAP220 decreases apical actin in a 3D mIMCD3 culture system – To test whether AKAP220 influenced formation of the actin barrier, we next moved to a 3-dimensional tissue culture model. For these experiments, mIMCD3 cells were cultured in Matrigel and allowed to spontaneously form 3D spheroids as described previously [108]. The lumen of these cysts is analogous to the lumen of the kidney collecting duct. We used the “clone 7” AKAP220 knockout line of mIMCD3 cells produced with CRISPR-Cas9 genome editing (described in Chapter 1) for these experiments (Fig. 4.6A). The cells were grown in Matrigel for 72 hours before fixation to allow the formation of small spheroids with defined lumens (Fig. 4.6B). We next stained the spheroids with phalloidin and compared apical actin thickness between WT and KO cells. Images were obtained by spinning disk confocal microscopy at 63X magnification. The actin signal is decreased at the apical membrane of AKAP220 knockout cysts, and is easily visualized with the application of a pixel intensity heatmap (Fig. 4.6 C). Although actin-rich structures still occur at sites of cell-cell contact in AKAP220 knockout spheroids (likely at tight junctions), the actin signal is reduced along the apical membrane. Representative surface plots of the indicated insets demonstrate this concept in 3D (Fig. 4.6D). The width of this apical actin signal was quantified and was significantly reduced in KO cells.

Together, these data provide strong preliminary data to support a role for AKAP220 in the production of the apical actin barrier. The decreased f-actin thickness observed in mIMCD3 cells is consistent with the urine phenotype observed in the mice.

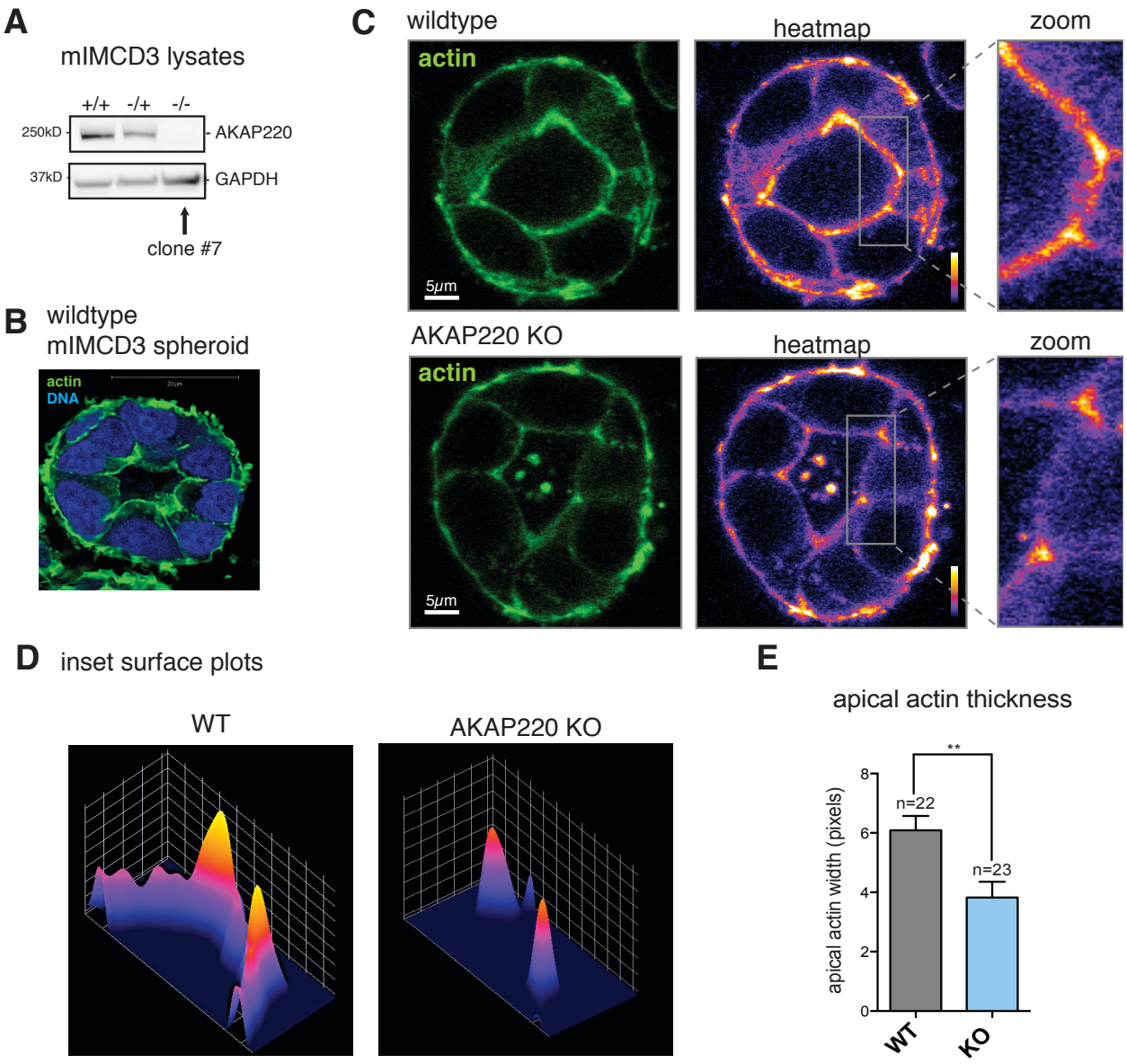

Figure 4.6 – Apical actin is decreased in AKAP220 knockout cells – A) Western blot analysis confirming loss of AKAP220 in the "clone 7" knockout line used for these experiments. B) Dilute single cell suspensions of mIMCD3 cells were grown in Matrigel for 72 hours to allow spontaneous growth of 3D spheroids. C) Spheroids were produced from WT or AKAP220 KO cell lines, fixed in 4% PFA, and stained with phalloidin to label f-actin. Cross sectional images were obtained at 63X magnification with spinning disk confocal microscopy, scale bars 5μm. Application of a pixel intensity heatmap aids the visualization of f-actin signal. Zoomed insets demonstrate a loss of apical actin signal in the AKAP220 knockout cells compared to wild-type. D) 3D surface plots of the boxed insets

CONCLUSIONS AND DISCUSSION

These studies introduce the first phenotypic analysis of the AKAP220 global knockout mouse. These animals have reduced body weight and length, but have normal food consumption relative to their size. They also have normal water intake and urinary output under *ad libitum* water conditions, and we therefore conclude that they do not have diabetes insipidus. Likewise, the dehydration response is intact in AKAP220 knockout animals, indicating the pathways controlling vasopressin synthesis, release, and responsiveness remain intact. These findings were surprising to us, as we originally hypothesized that AKAP220 might anchor the PKA required for vasopressin-responsive AQP2 translocation. However, based on this work it is likely that other AKAPs are responsible for regulating AQP2 trafficking during dehydration.

On the other hand, we had not considered how AKAPs might influence AQP2 during over-hydration. Both ends of this regulatory spectrum are required to maintain water homeostasis, yet less research has focused on how AQP2 is removed from the apical membrane when it is no longer needed. It is known that hypo-osmotic blood plasma inhibits vasopressin release, leading to internalization and degradation of AQP2 in the collecting ducts, therefore preventing water reabsorption. This allows excess water to be eliminated through the production of dilute urine, normalizing the blood osmolality. However, the mechanisms that govern and maintain AQP2 internalization during overhydration remain largely unknown.

Interestingly, we've found that AKAP220 global knockout mice do not respond normally to overhydration. The urine they produce following acute water loading is significantly more concentrated than wild-type animals, suggesting the AKAP220 knockouts are unable to efficiently eliminate excess water by diluting their urine. This indicated that AKAP220 might anchor signaling enzymes that contribute to water homeostasis in a pathway distinct from (but possibly complementary to) the vasopressin signaling cascade.

While investigating the molecular basis of the observed urine phenotype, we discovered that most AQP2 remains at the apical membrane in water-loaded AKAP220 knockout tissue. Because water transport through AQP2 is passive, apical membrane localization

is consistent with the observed decrease in urine diluting capacity. If AQP2 is inserted into the plasma membrane, water reabsorption will continue even during over-hydration because the interstitium of the kidney medulla is hyperosmotic by nature. The restricted staining pattern we observed in the AKAP220 knockout kidneys suggests that there is more AQP2 at the membrane, but future studies using immunogold labeling or surface biotinylation are warranted to confirm this hypothesis.

It is also interesting to note that we discover an increase in total AQP2 protein levels in AKAP220 knockout kidney lysates. This may be relevant to the localization of AQP2, as the half-life of this protein was previously shown to be longer when it was located in the plasma membrane than its half-life in vesicular membranes [85]. Whether the phosphorylation status of AQP2 has changed in the AKAP220 knockout kidneys remains to be explored. Inconclusive western blot data suggests that phosphorylation of Ser256 may be increased in the knockout, but this finding is confounded by the increase in total protein. However, as the total and phospho-signals both increased proportionately, we are inclined to think the primary driver for AQP2 mislocalization is not due to aberrant phosphorylation at AQP2-Ser256. Additionally, it is unlikely that AQP2 is mislocalized because it is no longer anchored by AKAP220 to the vesicular compartment. The baseline and dehydrated states show no change in vasopressin response, indicating that these shuttling mechanisms are intact in the absence of AKAP220.

Previous reports have found that basal fusion of AQP2-containing vesicles is prevented by a thick actin meshwork at the apical membrane of principal cells. This actin network is depolymerized in response to vasopressin stimulation, supporting the notion that it serves as a barrier to AQP2 translocation. The results described here suggest that AKAP220 anchors signaling molecules that promote the formation and/or maintenance of the actin barrier. This hypothesis is supported by previous work that has linked AKAP220 knockdown with decreased cortical actin and membrane ruffling *in vitro* [25].

The current literature indicates that RhoA is primarily responsible for creating the actin barrier. Although AKAP220 has never been shown to bind RhoA, we observe that RhoA is mislocalized in AKAP220 knockout kidneys in a manner similar to AQP2. In addition,

less GTP-bound RhoA is detected in crude lysates from water-loaded knockout animals. Therefore, the accumulation of AQP2 at the apical membrane could be caused by mislocalized and/or less active RhoA and a defective actin barrier. More experiments are necessary to determine whether AKAP220 is responsible for anchoring RhoA directly or through a binding partner, or whether it controls RhoA localization through upstream signaling. However, because RhoA controls formation of the actin barrier, we hypothesize that AKAP220 signaling complexes impact water homeostasis by upstream regulation of actin barrier production and maintenance.

Previous work from our lab has demonstrated that knocking down AKAP220 decreases cortical actin and membrane ruffling *in vitro*[25]. The 3D cell culture system in this work provides further support for this conclusion, and supports our hypothesis that AKAP220 influences actin barrier polymerization. Using CRISPR-Cas9 genome editing in mIMCD3 cells, we created a line that does not express AKAP220 ($AKAP220^{-/-}$). When grown in 3D culture, these cells form polarized spheroids with lumens analogous to the collecting duct lumen. We found that the width of the apical actin network was significantly reduced in the $AKAP220^{-/-}$ cells compared to wild-type cells. This provides further support that AKAP220 influences the cytoskeletal elements important for controlling AQP2 localization in the absence of vasopressin stimulation. This cell culture system will be useful in future efforts to determine the effects of treatments like vasopressin stimulation or hyper- or hypo-osmotic culture medium on actin barrier dimensions. In addition, it would be useful for studying chronic versus acute stimulation to help tease apart the signaling pathways involved in these mechanisms.

In conclusion, our work provides evidence that AKAP220 controls AQP2 localization in the absence of vasopressin stimulation. Whether AKAP220 is also involved in the vasopressin cascade remains to be seen, but we found no overt evidence of vasopressin malfunction in AKAP220 knockout animals. However, acute water loading experiments have unveiled a novel role for AKAP220 in controlling AQP2 during overhydration. Our evidence is consistent with defective actin barrier dynamics, and future experiments are necessary to determine exactly how the AKAP220 signaling complex controls this structure. Based on this work, it is likely that AKAP220 regulates upstream signaling events that promote RhoA activation in the absence of vasopressin

stimulation. Future experiments are needed to test this hypothesis, and to explore whether endocytic mechanisms such as AQP2 ubiquitination or dephosphorylation are intact in the AKAP220 knockout mice. In addition, exploring the role of AKAP220-anchored PP1 is an attractive candidate for future experiments.

In conclusion, we propose that AKAP220 anchors signaling enzymes to promote actin barrier stability and regulate AQP2 localization. Loss of AKAP220 leads to decreased apical actin thickness and causes AQP2 to accumulate at the membrane even during over-hydration. This phenotype is clinically relevant, as increasing AQP2 at the apical membrane is the desired outcome when treating patients with NDI. Therefore, elucidating the exact signaling pathways disrupted in AKAP220 knockout mice could reveal new therapeutic targets for this disease. Most cases of congenital NDI are caused by mutations in the vasopressin receptor. Therefore, pharmacologically activating downstream signaling enzymes to bypass the defective receptors could re-establish normal AQP2 translocation. Currently, very few treatment options exist for patients with congenital NDI, and most are relatively ineffective for easing symptoms. Therefore, our discovery that AKAP220 signaling complexes influence AQP2 localization provides preliminary and novel insight toward much needed therapeutic avenues for NDI treatment.

Experimental Procedures

Methods used in Chapter 2

Cell culture, transfection and lysis - HEK293 cells were maintained in DMEM supplemented with 10% FBS and penicillin/streptomycin, and mIMCD3 cells were maintained in DMEM:F12 1:1 media supplemented with 10% FBS and penicillin/streptomycin. Cells were transfected with plasmids using either Mirus TransIT-LT1 or Lipofectamine 2000 transfection reagents, and incubated for 48-72 hrs before fixation or lysis.

Co-immunoprecipitations – For pulldowns investigating the interaction with R subunit, cells were lysed in ice-cold buffer (20 mM HEPES, 150 mM NaCl, 5 mM EDTA, 1% triton, Pierce protease inhibitor cocktail). For pulldowns investigating the interaction with GSK3β and/or β-catenin, cells were washed in cold PBS and lysed in ice-cold lysis buffer (20 mM Tris-HCl pH 7.5, 150 mM NaCl, 1% Igepal, 5% glycerol, 25 mm β-glycerophosphate, 5 mm sodium orthovanadate, 5 mm NaF, 10 nM okadaic acid, and Pierce protease inhibitor cocktail). Cleared lysates were combined with primary antibody or flag-agarose beads and rocked at 4˚C for 1-4 hrs. Beads were washed 3X at 4˚C with lysis buffer and resuspended in sample buffer for SDS-PAGE and western blot analysis.

Peptide Array - A membrane-bound array of overlapping 20mer peptides spanning AKAP220 residues 1009-1305 was synthesized with an Intavis MultiPep array as described previously [109]. Membranes were overlayed with purified GSK3β, RI or RII at 4 ˚C overnight. GSK3β phosphorylation of candidate AKAP220 peptides was detected by *in vitro* kinase assay. Increasing concentrations of purified GSK3β (7.5 – 75 ng/µl) and a buffer containing [γ-^{32}P]ATP were incubated with the membrane-bound array of peptides and γ-^{32}P incorporation was detected by autoradiography.

CRISPR-Cas9 genome editing - The CRISPR/Cas9 expression vector pSpCas9(BB)-2A-GFP was obtained from the Zhang laboratory via Addgene (Addgene plasmid #48138) [110]. A 20-nucleotide sequence followed by a protospacer adjacent motif (PAM) from Streptococcus pyogenes of NGG targeting the second exon of mouse *Akap11* was selected using the Broad Institute online sgRNA designer

(http://www.broadinstitute.org/rnai/public/analysis-tools/sgrna-design) described by Doench et al 2014 [111]. The guide sequence was selected for the least number of potential off-target sites. The guide (sequence-PAM) was as follows (with a g in front necessary for the U6 promoter): 5'-GTCTTTAGGTGACTACTC CTGAGG-3'. The guide sequence without PAM was cloned into px458 as previously described [110].The plasmid was transfected into mIMDC3 cells by Lipofectamine 2000. Two days after transfection, single cells were sorted into 96-well plates by FACS. Two weeks after sorting, confluent clones were analyzed by genomic PCR using the following primers: 5´-AAGATTTTGCAGCTAAGGTGGC-3´and 5´-ACTACTTTCATACACGTTCGCCT-3´. PCR products were sequenced to identify changes in the genomic sequence. Loss of AKAP220 protein expression was further verified by western blot.

Immunostaining - Cells were seeded and transfected on 12 mm poly-D-lysine- and laminin-coated coverslips (Fisher Cat#: 08-774-385). To stimulate membrane ruffle formation, mIMCD3 cells were grown overnight on coverslips and treated with PDGF (50ng/ml) for 30min at 37˚C prior to fixation.

Cells fixed with 4% paraformaldehyde in PBS at room temperature for 10 min. Coverslips were blocked in PBS with 10% donkey serum for 2 hours at room temperature before primary antibody staining. Samples were washed 3x and incubated with donkey anti-mouse Alexafluor-488 and donkey anti-rabbit Alexafluor-555 secondary antibodies for 1 hr at room temperature. Three final washes were performed before mounting in ProLong Gold anti-fade reagent with DAPI (Invitrogen Cat #:P36935). Images were acquired by confocal microscopy with a 63X oil immersion objective.

Line plot analysis – Membrane ruffles were identified by morphology and positive f-actin staining at the plasma membrane (phalloidin). Line plots were drawn from outside the cell, perpendicular to the ruffle edge, through a region with actin signal. The pixel intensity across the line was quantified in ImageJ for >18 cells per experiment, n=3 experiments. Maximum projection images obtained with a 63X oil immersion objective.

Antibodies - Immunofluorescence and proximity ligation staining was done with mouse monoclonal anti-flag (Sigma cat #: F3165, FITC-conjugated cat#: F4049), rabbit polyclonal anti-RII (Santa Cruz sc-909) and polyclonal anti-RI (Santa Cruz sc-28893)

antibodies. Co-immunoprecipitations were achieved with flag-agarose beads (Sigma cat#: A2220), cAMP agarose beads (BioLog cat#: A020-06), mouse monoclonal anti-V5 (Life Technologies cat #: R96025), and rabbit anti-GFP (Life Technologies cat #: 11122). Immunoblots were probed with mouse monoclonal anti-RII (BD cat#: 610626), mouse monoclonal anti-GSK3β (BD cat#: 610201), mouse monoclonal anti-β-catenin (BD cat#: 610154), or rabbit monoclonal anti-phospho-GSK3β(Ser9) (Millipore cat#:04-1075) and rabbit polyclonal anti-AKAP220 produced by our lab. Membrane ruffling experiments were perforumed using Molecular Probes Actin-488 (Invitrogen), mouse monoclonal anti-β-catenin (BD) and rabbit polyclonal anti-GSK3β (Cell Signaling cat#: 12456P). Peptide array and purified protein overlays were probed with purified biotin-RII or biotin-RI and detected with Neutravidin-HRP (Life Technologies cat#: 31030).

Fluorescence polarization- FITC-labeled peptides were synthesized to >95% purity by BioMatik and resuspended to 100 μM stocks in assay buffer (20 mM HEPES pH 7.5, 200 mM NaCl, and 0.1% triton X-100). Assay performed in black, round bottomed 96-well plates (Corning Cat #: 3792). FITC-peptides were diluted to 5 nM final concentration in assay buffer and combined with varying concentrations of purified His-RII at a total volume of 100 μl per well. Fluorescence polarization measurements were made using a POLARstar Omega plate reader (BMG Labtech) and converted to anisotropy values. Binding data was fit using non-linear regression to a one-site binding model in GraphPad Prism 6.0 (Fluorescence polarization = Bmax * [RIIα] / (Kd+RIIα) + NS * RIIα + Background). In this equation, Bmax is the maximum specific binding, Kd is the equilibrium constant, NS is the slope of non-specific binding and Background is the amount of fluorescence polarization of each FITC-peptide with no RII added.

Duolink Proximity Ligation Assays - Cells were seeded onto acid-washed glass coverslips and transfected. They were fixed in 4% PFA and stained according to the Duolink proximity ligation assay protocol. Before mounting, the cells were counterstained with a FITC-anti-flag antibody (Sigma cat#: F4049) to identify transfected cells. Images were obtained by confocal microscopy with a 63X oil immersion objective. For quantification of puncta, ImageJ was used to outline FITC-positive cells. The number of puncta in this region of interest (ROI) was counted with the

"find maxima" algorithm [44]. To subtract background, this exact ROI was moved to a region containing FITC-negative cells and the number of puncta counted.

Methods used in Chapter 3

Knockout vector production - The knockout vector was generated using a Bacmid ordered from the Children's Hospital Oakland Research Institute (clone RP23-239B21). Vega Biolabs engineered a retrieval plasmid containing arms of homology flanking the target sequence to capture approximately 14kb of the genomic *Akap11* locus. LoxP sites were added to the intronic regions surrounding Exons 6 and 7. Within this "floxed" region, a Neo cassette flanked by two Frt sites was inserted for positive selection of ES cell clones. The Frt sites were included to allow removal of the Neo gene at a later stage by breeding with mice expressing FLP recombinase. Because cells are more likely incorporate DNA randomly into the genome rather than through homologous recombination, a herpes virus thymidine kinas (*HSV-TK*I) cassette was included in the vector backbone as negative selection marker, outside of the *Akap11* genomic sequence. ES cell clones were grown in the presence of Fialuridine (FIAU), a thymidine analog that kills cells expressing the *HSV-TK* gene but not endogenous thymidine kinase. This allowed for removal of clones that incorporated the vector through random insertion and increased the likelihood of identifying clones of interest. Finally, the knockout vector was designed to contain new cut sites for BamHI and StuI for Southern blot analysis. Incorporation of these sites into the genomic DNA would be detected by a band shift using Southern blot probes designed within the *Akap11* gene.

ES cell electroporation – The knockout vector was digested overnight with I-CeuI at 37˚C. The I-CeuI recognition sequence (5'-TAACTATAACGGTCCTAA^GGTAGCGAA-3') occurs only once in the backbone of the knockout vector, outside of the captured *Akap11* genomic region. This DNA was given to the University of Washington Transgenics Resources Program for electroporation into mouse embryonic stem (ES) cells. We used the G4 hybrid ES line produced by 129S6/SvEvTac and C57BL/6Ncr mice. Cells were electroporated and grown in the presence of G418 to select for clones that had incorporated the Neo cassette from the knockout vector.

PCR Screening - ES cells were lysed in lysis buffer (10 mM Tris-HCl, pH 7.5, 10 mM EDTA, 10 mM NaCl, 0.5% SDS, 250 µg/ml Proteinase K) and DNA was purified by phenol-choloroform extraction. As an initial screen for homologous recombination events, PCR primers were designed to flank the 3' loxP site. (LoxP forward primer: 5'-GAC AAA TGC TGG GCA TGC TGT TAG CAG G-3', LoxP reverse primer: 5' CAA GCT TAA GGA AGA CTG CGG GGT AC-3'). The wild-type genomic sequence would produce a PCR product of 579bp, while the presence of a loxP site between the primers would create a product of 657bp. The StuI site engineered just downstream of the loxP site provided additional confirmation of PCR products by restriction digest.

Southern Blot – Overnight BamHI or StuI digests were performed on purified DNA from candidate clones. The digested DNA was run onto large format 1% agatrose gels containing ethidium bromide and the digestion efficiency was visualized by UV light. The gel was first depurinated in 0.25 M HCl, then denatured in 0.5 M NaOH and 1.5 M NaCl. Finally, the gel was neutralized in 1 M Tris pH 7.0 and 1.5 M NaCl.

The digested DNA was transferred overnight onto nylon GeneScreen hybridization membranes by capillary action in 10X SSC (1.5 M NaCl, 150 mM sodium citrate, pH 7.0). The membrane was washed in denaturing buffer (0.4 N NaOH) and then neutralized (0.2 M Tris pH 7.0, 1X SSC). The DNA was crosslinked to the membrane with ultraviolet light and prepared for the Southern blot by rehydrating in pre-warmed hybridization buffer (UltraHyb, Life Technologies Cat #: AM8670).

The BamHI and StuI Southern blot probes were produced by PCR from genomic template DNA, gel purified, and radiolabeled with [α-32P]-ATP. The labeled probes were denatured at 95˚C and added to the pre-warmed membrane in hybridization buffer. The membranes were incubated overnight in a rotating hybridization oven at 42˚C. They were washed 2x5min in pre-heated low-stringency buffer (2X SSC, 0.1% SDS) and 2x15min in high-stringency buffer (0.1% SSC, 0.1% SDS). The membranes were placed between sheets of plastic film and exposed to film for 3 days at -80˚C.

For the BamHI probe, a band was expected at 13.0 kb, corresponding to the wild-type allele. If the 5' arm of the knockout vector incorporated by homologous recombination, a second band would be visible at 8.3 kb. Likewise for the StuI probe, a wild-type band

was expected at 18.4 kb and if the 3' arm of the knockout vector was incorporated by homologous recombination a second band would be visible at 9.3 kb.

Chimera Production – ES cell clones #42 and #70 were confirmed positive for homologous recombination by both PCR and Southern Blot analysis. These clones were then thawed and expanded by the University of Washington Transgenics Resources Program. The cells were microinjected into C57Bl/6J blastocysts and implanted into pseudopregnant female mice. Chimeric mice were identified by the presence of agouti versus black coat coloring. All chimeric offspring were bred to C57Bl/6J and tested for germline transmission of the floxed *Akap11* allele by PCR analysis.

FRT-FLP and Cre-lox breeding – The Frt-flanked Neo cassette was removed from the genome by crossing to mice expressing FLP recombinase (B6(C3)-Tg(Pgk1-FLPo)10Sykr/J). Offspring were screened for both the FLP transgene and the Neo cassette to confirm efficient collapse of the Frt sites. After deletion of the Neo cassette was confirmed, global knockout mice were produced by crossing *Akap11*$^{lox/lox}$ animals with mice expressing cre recombinase under the control of the EIIa adenoviral promoter (B6.FVB-Tg(EIIa-cre)C5379Lmgd/J). Offspring were screened for the Cre transgene and the wild-type, floxed, or collapsed *Akap11* alleles.

Genotyping – A primer pair flanking the 3' loxP site was designed for genotyping the floxed *Akap11* allele (LoxP forward primer: 5'-GAC AAA TGC TGG GCA TGC TGT TAG CAG G-3', LoxP reverse primer: 5' CAA GCT TAA GGA AGA CTG CGG GGT AC-3'). A wild-type allele produces a 579 bp product while the floxed allele produces a 657 bp product. The PCR products were run onto 1% TBE agarose gels for detection.

A second PCR primer pair was designed to detect loxP collapse in *Akap11*$^{-/-}$ mice. These primers anneal outside the loxP sites and only produce a product if the allele has collapsed. To fully genotype the global knockout animals, both the wild-type and collapsed PCR reactions are required. Heterozygous animals have PCR products present in both reactions, while homozygotes are positive for only the wild-type or collapsed allele.

Methods used in Chapter 4

Metabolic cages – Tecniplast™ metabolic rodent cages equipped with detachable water bottles and food hoppers were used for these experiments. Mice were provided with the mash/crumble form of LabDiet 5053. To acclimate to the environment and the non-pellet food format, mice were housed individually in the metabolic cages for 4 days prior to the experiment. During this time, the water bottle and food hoppers were refilled and the urine and feces collection cups emptied daily. To prevent evaporation, the urine collection cup was filled with 1ml mineral oil each day. The water bottle, food hopper, and urine and feces collection cups from each cage were weighed every 24 hours for 3 days. The total body weight of each mouse was also recorded to allow normalization of each parameter as a percent of body weight.

Tissue lysis and western blots – Kidneys were harvested and microdissected to separate cortex and medulla. The tissue was lysed in ice cold RIP buffer (50mM Tris-HCl, pH 8.0, 150mM NaCl, 1% NP40, 0.5% sodium deoxycholate, 0.1% SDS, protease inhibitor cocktail) using a handheld BioVortexer (Research Products International, cat#: 141290). Lysates were cleared by centrifugation. For western blot analysis, samples were run onto SDS-PAGE gels, transferred to nitrocellulose and blocked in 5% milk. Membranes were incubated with primary antibodies overnight at 4˚C.

Quantitative PCR – The mRNA was isolated from fresh kidney medulla lysates with a Qiagen RNeasy kit (Qiagen, cat#: 74104) and reverse transcribed into cDNA with the BioRad iScript cDNA Synthesis kit (BioRad, cat#: 170-8890). TaqMan probes for AQP2 and GAPDH were obtained from Life Technologies (cat#: 4331182 and 4331182, respectively). Reactions were run and analyzed on the Applied Biosystems Prism 7700 Sequence Detection System using version 1.6 software.

Dehydration and water loading – Animals were dehydrated by complete removal of water access for 24 hours in the home cage. Animals were water loaded with 10% glucose in water (3% total body weight) through a blunt ended stainless steel oral gavage needle. These animals were allowed to recover for 30min in the home cage prior to placing into the urine collection cages. When they were transferred to the urine

collection cages, the animals were scruffed to encourage bladder voiding and ensure all samples produced in the collection cage were representative of the water-loaded state.

Urine osmolality measurements – Urine samples were collected from animals placed into individual boxes lined with plastic 96-well plates. Samples were collected by pipette and stored at -20˚C. Osmolality measurements were made with a Vapro^{TM} vapor pressure osmometer (model #5520) calibrated with Wescor Opti-Mole osmolality standards (100mmol/kg, 290mmol/kg, 1000mmol/kg). Urine samples from dehydrated animals were diluted to keep the reading within the linear detection range of the device. 10µl of diluted urine was pipetted onto a paper disc, inserted into the equilibrated osmometer, and readings recorded. Samples were read in triplicate and averaged.

Paraffin embedded tissue staining – Kidneys were harvested and fixed in 10% buffered formalin at 4˚C for three days. Samples were sent to the UW Histology Core, embedded in paraffin and sliced into 4µm thick sections onto glass slides. Samples were deparaffinized with Citrasolv (Fisher, cat#: 12-518-213) and dehydrated in subsequent baths of 100%, 95%, 85%, and 70% ethanol. Samples were then rinsed in ddH2O for 2min prior to antigen retrieval. Slides were submerged in Buffer A (Electron Microscopy Sciences, cat#: 62706-10) and placed into a Retriever 2100 pressure cooker (Electron Microscopy Sciences). Following completion of the antigen retrival protocol, slides were left to cool overnight. The following day, tissue sections were circled with Pap-Pen and covered with block buffer (10% donkey serum and 1% fish gelatin in PBS) for 2 hours at room temperature. Sections were incubated with primary antibodies overnight at 4˚C, washed 3 times in PBS, and incubated 1hr at room temperature in Alexafluor 2˚ antibodies. Tissue sections were mounted under glass coverslips in ProLong Gold mounting media (LifeTech Cat #P36931). For long-term storage, slides were kept in a dark slide chamber at -20˚C.

Line plot analysis – Localization of proteins was assessed by line plot analysis in ImageJ software. Lines were drawn starting from the lumen of the collecting duct, perpendicular to the apical plasma membrane. The lines were drawn only through cells with a visible nucleus in the focal plane, and line placement was through the cytosol

adjacent to the nucleus. Pixel intensity was measured for one line per principal cell, and the start of the apical membrane was aligned for all line plots.

Rhotekin pulldown assay – Kidneys were harvested from mice, microdissected to isolate the medulla, and lysed in ice-cold RIPA buffer. The cleared lysate was combined with GST-tagged Rhotekin-RBD protein conjugated to agarose beads according to the manufacturer instructions (Cytoskeleton, Inc., cat#: BK-036). Samples were washed and run out for western blot analysis. The ratio of GTP-bound RhoA (from the bead pulldown) was compared to the input total RhoA (from the lysate) for each individual sample to normalize for differences in protein input. The ratio values were then compared between wild-type and knockout tissue.

mIMCD3 spheroid production – For spheroid formation, mIMCD3 cells were cultured in 50% Matrigel and 50% DMEM:F12 media supplemented with 10% FBS and pen/strep as described previously [108]. Cells were grown for 72 hours prior to fixation in 4% PFA for 1 hour at room temperature with gentle shaking. Spheroids were permeabilized with 0.1% PBST and blocked in PBS with 5% donkey serum. Phalloidin and DRAQ5 stains were performed at room temperature for 30min. Cells were washed 3X in PBS and mounted in Vectashield (Vector Labs, cat#: H-1000). Cross sectional images of the spheroids were acquired at 63X by spinning disk confocal microscopy. Only spheroids with visible, open lumens were included in analysis of apical actin thickness.

References

1. Berg, J. M. T., J.L.; Stryer. L. *Biochemistry: Chapter 15, Signal-Transduction Pathways: An Introduction to Information Metabolism*. 5th Edition. (2002).

2. Rojas, A. M., Fuentes, G., Rausell, A. & Valencia, A. The Ras protein superfamily: evolutionary tree and role of conserved amino acids. *The Journal of cell biology* **196**, 189-201, doi:10.1083/jcb.201103008 (2012).

3. Bauman, A. L. & Scott, J. D. Kinase- and phosphatase-anchoring proteins: harnessing the dynamic duo. *Nature cell biology* **4**, E203-206, doi:10.1038/ncb0802-e203 (2002).

4. Wong, W. & Scott, J. D. AKAP signalling complexes: focal points in space and time. *Nature reviews. Molecular cell biology* **5**, 959-970, doi:10.1038/nrm1527 (2004).

5. Good, M. C., Zalatan, J. G. & Lim, W. A. Scaffold proteins: hubs for controlling the flow of cellular information. *Science* **332**, 680-686, doi:10.1126/science.1198701 (2011).

6. Welch, E. J., Jones, B. W. & Scott, J. D. Networking with AKAPs: context-dependent regulation of anchored enzymes. *Molecular interventions* **10**, 86-97, doi:10.1124/mi.10.2.6 (2010).

7. Gold, M. G. *et al.* Molecular basis of AKAP specificity for PKA regulatory subunits. *Molecular cell* **24**, 383-395, doi:10.1016/j.molcel.2006.09.006 (2006).

8. Carlson, C. R. *et al.* Delineation of type I protein kinase A-selective signaling events using an RI anchoring disruptor. *The Journal of biological chemistry* **281**, 21535-21545, doi:10.1074/jbc.M603223200 (2006).

9. Wong, W., Goehring, A. S., Kapiloff, M. S., Langeberg, L. K. & Scott, J. D. mAKAP compartmentalizes oxygen-dependent control of HIF-1alpha. *Science signaling* **1**, ra18, doi:10.1126/scisignal.2000026 (2008).

10. Asirvatham, A. L. *et al.* A-kinase anchoring proteins interact with phosphodiesterases in T lymphocyte cell lines. *Journal of immunology* **173**, 4806-4814 (2004).

11. Bauman, A. L. *et al.* Dynamic regulation of cAMP synthesis through anchored PKA-adenylyl cyclase V/VI complexes. *Molecular cell* **23**, 925-931, doi:10.1016/j.molcel.2006.07.025 (2006).

12. Hinke, S. A. *et al.* Anchored phosphatases modulate glucose homeostasis. *The EMBO journal* **31**, 3991-4004, doi:10.1038/emboj.2012.244 (2012).

13. Navedo, M. F. *et al.* AKAP150 is required for stuttering persistent Ca2+ sparklets and angiotensin II-induced hypertension. *Circulation research* **102**, e1-e11, doi:10.1161/CIRCRESAHA.107.167809 (2008).

14. Taylor, S. S., Ilouz, R., Zhang, P. & Kornev, A. P. Assembly of allosteric macromolecular switches: lessons from PKA. *Nature reviews. Molecular cell biology* **13**, 646-658, doi:10.1038/nrm3432 (2012).

15. Knighton, D. R. *et al.* Crystal structure of the catalytic subunit of cyclic adenosine monophosphate-dependent protein kinase. *Science* **253**, 407-414 (1991).

16. Su, Y. *et al.* Regulatory subunit of protein kinase A: structure of deletion mutant with cAMP binding domains. *Science* **269**, 807-813 (1995).

17. Kinderman, F. S. *et al.* A dynamic mechanism for AKAP binding to RII isoforms of cAMP-dependent protein kinase. *Molecular cell* **24**, 397-408, doi:10.1016/j.molcel.2006.09.015 (2006).

18. Carr, D. W. *et al.* Interaction of the regulatory subunit (RII) of cAMP-dependent protein kinase with RII-anchoring proteins occurs through an amphipathic helix binding motif. *The Journal of biological chemistry* **266**, 14188-14192 (1991).

19. Newlon, M. G. *et al.* A novel mechanism of PKA anchoring revealed by solution structures of anchoring complexes. *The EMBO journal* **20**, 1651-1662, doi:10.1093/emboj/20.7.1651 (2001).

20. Smith, F. D. *et al.* Intrinsic disorder within an AKAP-protein kinase A complex guides local substrate phosphorylation. *eLife* **2**, e01319, doi:10.7554/eLife.01319 (2013).

21. Dessauer, C. W. Adenylyl cyclase--A-kinase anchoring protein complexes: the next dimension in cAMP signaling. *Molecular pharmacology* **76**, 935-941, doi:10.1124/mol.109.059345 (2009).

22. Lester, L. B., Coghlan, V. M., Nauert, B. & Scott, J. D. Cloning and characterization of a novel A-kinase anchoring protein. AKAP 220, association with testicular peroxisomes. *The Journal of biological chemistry* **271**, 9460-9465 (1996).

23. Tanji, C. *et al.* A-kinase anchoring protein AKAP220 binds to glycogen synthase kinase-3beta (GSK-3beta) and mediates protein kinase A-dependent inhibition

of GSK-3beta. *The Journal of biological chemistry* **277**, 36955-36961, doi:10.1074/jbc.M206210200 (2002).

24. Schillace, R. V. & Scott, J. D. Association of the type 1 protein phosphatase PP1 with the A-kinase anchoring protein AKAP220. *Current biology : CB* **9**, 321-324 (1999).

25. Logue, J. S., Whiting, J. L., Tunquist, B., Langeberg, L. K. & Scott, J. D. Anchored protein kinase A recruitment of active Rac GTPase. *The Journal of biological chemistry* **286**, 22113-22121, doi:10.1074/jbc.M111.232660 (2011).

26. Logue, J. S. *et al.* AKAP220 protein organizes signaling elements that impact cell migration. *The Journal of biological chemistry* **286**, 39269-39281, doi:10.1074/jbc.M111.277756 (2011).

27. Okutsu, R. *et al.* AKAP220 colocalizes with AQP2 in the inner medullary collecting ducts. *Kidney international* **74**, 1429-1433, doi:10.1038/ki.2008.402 (2008).

28. Frame, S., Cohen, P. & Biondi, R. M. A common phosphate binding site explains the unique substrate specificity of GSK3 and its inactivation by phosphorylation. *Molecular cell* **7**, 1321-1327 (2001).

29. Logue, J. S., Whiting, J. L. & Scott, J. D. Sequestering Rac with PKA confers cAMP control of cytoskeletal remodeling. *Small GTPases* **2**, 173-176, doi:10.4161/sgtp.2.3.16487 (2011).

30. Watanabe, T. *et al.* Interaction with IQGAP1 links APC to Rac1, Cdc42, and actin filaments during cell polarization and migration. *Developmental cell* **7**, 871-883, doi:10.1016/j.devcel.2004.10.017 (2004).

31. Watanabe, T. *et al.* Phosphorylation of CLASP2 by GSK-3beta regulates its interaction with IQGAP1, EB1 and microtubules. *Journal of cell science* **122**, 2969-2979, doi:10.1242/jcs.046649 (2009).

32. Schillace, R. V., Voltz, J. W., Sim, A. T., Shenolikar, S. & Scott, J. D. Multiple interactions within the AKAP220 signaling complex contribute to protein phosphatase 1 regulation. *The Journal of biological chemistry* **276**, 12128-12134, doi:10.1074/jbc.M010398200 (2001).

33. Kuwahara, M. *et al.* cAMP-dependent phosphorylation stimulates water permeability of aquaporin-collecting duct water channel protein expressed in Xenopus oocytes. *The Journal of biological chemistry* **270**, 10384-10387 (1995).

34. Rao, R., Patel, S., Hao, C., Woodgett, J. & Harris, R. GSK3beta mediates renal response to vasopressin by modulating adenylate cyclase activity. *Journal of the American Society of Nephrology : JASN* **21**, 428-437, doi:10.1681/ASN.2009060672 (2010).

35. Moeller, H. B., Aroankins, T. S., Slengerik-Hansen, J., Pisitkun, T. & Fenton, R. A. Phosphorylation and ubiquitylation are opposing processes that regulate endocytosis of the water channel aquaporin-2. *Journal of cell science* **127**, 3174-3183, doi:10.1242/jcs.150680 (2014).

36. Fang, X. *et al.* Phosphorylation and inactivation of glycogen synthase kinase 3 by protein kinase A. *Proceedings of the National Academy of Sciences of the United States of America* **97**, 11960-11965, doi:10.1073/pnas.220413597 (2000).

37. Obenauer, J. C., Cantley, L. C. & Yaffe, M. B. Scansite 2.0: Proteome-wide prediction of cell signaling interactions using short sequence motifs. *Nucleic acids research* **31**, 3635-3641 (2003).

38. Burns-Hamuro, L. L. *et al.* Designing isoform-specific peptide disruptors of protein kinase A localization. *Proceedings of the National Academy of Sciences of the United States of America* **100**, 4072-4077, doi:10.1073/pnas.2628038100 (2003).

39. Gold, M. G. *et al.* Engineering A-kinase anchoring protein (AKAP)-selective regulatory subunits of protein kinase A (PKA) through structure-based phage selection. *The Journal of biological chemistry* **288**, 17111-17121, doi:10.1074/jbc.M112.447326 (2013).

40. Burgers, P. P., van der Heyden, M. A., Kok, B., Heck, A. J. & Scholten, A. A systematic evaluation of protein kinase A-A-kinase anchoring protein interaction motifs. *Biochemistry* **54**, 11-21, doi:10.1021/bi500721a (2015).

41. Kovanich, D. *et al.* Sphingosine kinase interacting protein is an A-kinase anchoring protein specific for type I cAMP-dependent protein kinase. *Chembiochem : a European journal of chemical biology* **11**, 963-971, doi:10.1002/cbic.201000058 (2010).

42. Burgers, P. P. *et al.* A small novel A-kinase anchoring protein (AKAP) that localizes specifically protein kinase A-regulatory subunit I (PKA-RI) to the plasma membrane. *The Journal of biological chemistry* **287**, 43789-43797, doi:10.1074/jbc.M112.395970 (2012).

43. Alto, N. M. *et al.* Bioinformatic design of A-kinase anchoring protein-in silico: a potent and selective peptide antagonist of type II protein kinase A anchoring. *Proceedings of the National Academy of Sciences of the United States of America* **100**, 4445-4450, doi:10.1073/pnas.0330734100 (2003).

44. Gajadhar, A. & Guha, A. A proximity ligation assay using transiently transfected, epitope-tagged proteins: application for in situ detection of dimerized receptor tyrosine kinases. *BioTechniques* **48**, 145-152, doi:10.2144/000113354 (2010).

45. Westphal, R. S. *et al.* Regulation of NMDA receptors by an associated phosphatase-kinase signaling complex. *Science* **285**, 93-96 (1999).

46. Witczak, O. *et al.* Cloning and characterization of a cDNA encoding an A-kinase anchoring protein located in the centrosome, AKAP450. *The EMBO journal* **18**, 1858-1868, doi:10.1093/emboj/18.7.1858 (1999).

47. Means, C. K. *et al.* An entirely specific type I A-kinase anchoring protein that can sequester two molecules of protein kinase A at mitochondria. *Proceedings of the National Academy of Sciences of the United States of America* **108**, E1227-1235, doi:10.1073/pnas.1107182108 (2011).

48. Amieux, P. S. & McKnight, G. S. The essential role of RI alpha in the maintenance of regulated PKA activity. *Annals of the New York Academy of Sciences* **968**, 75-95 (2002).

49. Brandon, E. P., Idzerda, R. L. & McKnight, G. S. PKA isoforms, neural pathways, and behaviour: making the connection. *Current opinion in neurobiology* **7**, 397-403 (1997).

50. Hernandez, F., Langa, E., Cuadros, R., Avila, J. & Villanueva, N. Regulation of GSK3 isoforms by phosphatases PP1 and PP2A. *Molecular and cellular biochemistry* **344**, 211-215, doi:10.1007/s11010-010-0544-0 (2010).

51. Emes, R. D., Goodstadt, L., Winter, E. E. & Ponting, C. P. Comparison of the genomes of human and mouse lays the foundation of genome zoology. *Human molecular genetics* **12**, 701-709 (2003).

52. Nguyen, D. & Xu, T. The expanding role of mouse genetics for understanding human biology and disease. *Disease models & mechanisms* **1**, 56-66, doi:10.1242/dmm.000232 (2008).

53. Agre, P. *et al.* Aquaporin CHIP: the archetypal molecular water channel. *The American journal of physiology* **265**, F463-476 (1993).

54. Gonen, T., Sliz, P., Kistler, J., Cheng, Y. & Walz, T. Aquaporin-0 membrane junctions reveal the structure of a closed water pore. *Nature* **429**, 193-197, doi:10.1038/nature02503 (2004).

55. Nielsen, S. *et al.* Aquaporins in the kidney: from molecules to medicine. *Physiological reviews* **82**, 205-244, doi:10.1152/physrev.00024.2001 (2002).

56. Stevens, L. A., Coresh, J., Greene, T. & Levey, A. S. Assessing kidney function--measured and estimated glomerular filtration rate. *The New England journal of medicine* **354**, 2473-2483, doi:10.1056/NEJMra054415 (2006).

57. Bertram, J. F., Douglas-Denton, R. N., Diouf, B., Hughson, M. D. & Hoy, W. E. Human nephron number: implications for health and disease. *Pediatric nephrology* **26**, 1529-1533, doi:10.1007/s00467-011-1843-8 (2011).

58. Ronco, C., Bellomo, R. & Ricci, Z. Hemodynamic response to fluid withdrawal in overhydrated patients treated with intermittent ultrafiltration and slow continuous ultrafiltration: role of blood volume monitoring. *Cardiology* **96**, 196-201 (2001).

59. Jacobson, H. R. & Seldin, D. W. Proximal tubular reabsorption and its regulation. *Annual review of pharmacology and toxicology* **17**, 623-646, doi:10.1146/annurev.pa.17.040177.003203 (1977).

60. Maunsbach, A. B. *et al.* Aquaporin-1 water channel expression in human kidney. *Journal of the American Society of Nephrology : JASN* **8**, 1-14 (1997).

61. Nielsen, S. *et al.* Aquaporin-1 water channels in short and long loop descending thin limbs and in descending vasa recta in rat kidney. *The American journal of physiology* **268**, F1023-1037 (1995).

62. Mount, D. B. Thick ascending limb of the loop of Henle. *Clinical journal of the American Society of Nephrology : CJASN* **9**, 1974-1986, doi:10.2215/CJN.04480413 (2014).

63. Gottschalk, C. W. & Mylle, M. Evidence that the mammalian nephron functions as a countercurrent multiplier system. *Science* **128**, 594 (1958).

64. Kortenoeven, M. L. & Fenton, R. A. Renal aquaporins and water balance disorders. *Biochimica et biophysica acta* **1840**, 1533-1549, doi:10.1016/j.bbagen.2013.12.002 (2014).

65. Pearce, D. *et al.* Collecting duct principal cell transport processes and their regulation. *Clinical journal of the American Society of Nephrology : CJASN* **10**, 135-146, doi:10.2215/CJN.05760513 (2015).

66. van Balkom, B. W. *et al.* Role of cytoplasmic termini in sorting and shuttling of the aquaporin-2 water channel. *American journal of physiology. Cell physiology* **286**, C372-379, doi:10.1152/ajpcell.00271.2003 (2004).

67. Hoffert, J. D., Pisitkun, T., Wang, G., Shen, R. F. & Knepper, M. A. Quantitative phosphoproteomics of vasopressin-sensitive renal cells: regulation of aquaporin-2 phosphorylation at two sites. *Proceedings of the National Academy of Sciences*

of the United States of America **103**, 7159-7164, doi:10.1073/pnas.0600895103 (2006).

68. Sands, J. M. & Layton, H. E. The physiology of urinary concentration: an update. *Seminars in nephrology* **29**, 178-195, doi:10.1016/j.semnephrol.2009.03.008 (2009).

69. Eknoyan, G. A history of diabetes insipidus: paving the road to internal water balance. *American journal of kidney diseases : the official journal of the National Kidney Foundation* **56**, 1175-1183, doi:10.1053/j.ajkd.2010.08.002 (2010).

70. Fujiwara, T. M., Morgan, K. & Bichet, D. G. Molecular biology of diabetes insipidus. *Annual review of medicine* **46**, 331-343, doi:10.1146/annurev.med.46.1.331 (1995).

71. Knoers, N. & Monnens, L. A. Nephrogenic diabetes insipidus: clinical symptoms, pathogenesis, genetics and treatment. *Pediatric nephrology* **6**, 476-482 (1992).

72. Fujimoto, M. *et al.* Clinical overview of nephrogenic diabetes insipidus based on a nationwide survey in Japan. *Yonago acta medica* **57**, 85-91 (2014).

73. Fujiwara, T. M. & Bichet, D. G. Molecular biology of hereditary diabetes insipidus. *Journal of the American Society of Nephrology : JASN* **16**, 2836-2846, doi:10.1681/ASN.2005040371 (2005).

74. Maghnie, M. *et al.* Central diabetes insipidus in children and young adults. *The New England journal of medicine* **343**, 998-1007, doi:10.1056/NEJM200010053431403 (2000).

75. Maghnie, M. *et al.* Idiopathic central diabetes insipidus in children and young adults is commonly associated with vasopressin-cell antibodies and markers of autoimmunity. *Clinical endocrinology* **65**, 470-478, doi:10.1111/j.1365-2265.2006.02616.x (2006).

76. Rosenthal, W. *et al.* Mutations in the vasopressin V2 receptor gene in families with nephrogenic diabetes insipidus and functional expression of the Q-2 mutant. *Cellular and molecular biology* **40**, 429-436 (1994).

77. Birnbaumer, M. Vasopressin receptor mutations and nephrogenic diabetes insipidus. *Archives of medical research* **30**, 465-474 (1999).

78. Sands, J. M., Bichet, D. G., American College of, P. & American Physiological, S. Nephrogenic diabetes insipidus. *Annals of internal medicine* **144**, 186-194 (2006).

79. Loffing, J. Paradoxical antidiuretic effect of thiazides in diabetes insipidus: another piece in the puzzle. *Journal of the American Society of Nephrology : JASN* **15**, 2948-2950, doi:10.1097/01.ASN.0000146568.82353.04 (2004).

80. Katsura, T., Gustafson, C. E., Ausiello, D. A. & Brown, D. Protein kinase A phosphorylation is involved in regulated exocytosis of aquaporin-2 in transfected LLC-PK1 cells. *The American journal of physiology* **272**, F817-822 (1997).

81. Fenton, R. A. *et al.* Acute regulation of aquaporin-2 phosphorylation at Ser-264 by vasopressin. *Proceedings of the National Academy of Sciences of the United States of America* **105**, 3134-3139, doi:10.1073/pnas.0712338105 (2008).

82. Hoffert, J. D. *et al.* Vasopressin-stimulated increase in phosphorylation at Ser269 potentiates plasma membrane retention of aquaporin-2. *The Journal of biological chemistry* **283**, 24617-24627, doi:10.1074/jbc.M803074200 (2008).

83. Hoffert, J. D. *et al.* Dynamics of aquaporin-2 serine-261 phosphorylation in response to short-term vasopressin treatment in collecting duct. *American journal of physiology. Renal physiology* **292**, F691-700, doi:10.1152/ajprenal.00284.2006 (2007).

84. van Balkom, B. W. *et al.* The role of putative phosphorylation sites in the targeting and shuttling of the aquaporin-2 water channel. *The Journal of biological chemistry* **277**, 41473-41479, doi:10.1074/jbc.M207525200 (2002).

85. Moeller, H. B., Praetorius, J., Rutzler, M. R. & Fenton, R. A. Phosphorylation of aquaporin-2 regulates its endocytosis and protein-protein interactions. *Proceedings of the National Academy of Sciences of the United States of America* **107**, 424-429, doi:10.1073/pnas.0910683107 (2010).

86. Nejsum, L. N., Zelenina, M., Aperia, A., Frokiaer, J. & Nielsen, S. Bidirectional regulation of AQP2 trafficking and recycling: involvement of AQP2-S256 phosphorylation. *American journal of physiology. Renal physiology* **288**, F930-938, doi:10.1152/ajprenal.00291.2004 (2005).

87. Moeller, H. B., MacAulay, N., Knepper, M. A. & Fenton, R. A. Role of multiple phosphorylation sites in the COOH-terminal tail of aquaporin-2 for water transport: evidence against channel gating. *American journal of physiology. Renal physiology* **296**, F649-657, doi:10.1152/ajprenal.90682.2008 (2009).

88. Eto, K., Noda, Y., Horikawa, S., Uchida, S. & Sasaki, S. Phosphorylation of aquaporin-2 regulates its water permeability. *The Journal of biological chemistry* **285**, 40777-40784, doi:10.1074/jbc.M110.151928 (2010).

89. Valenti, G. *et al.* The phosphatase inhibitor okadaic acid induces AQP2 translocation independently from AQP2 phosphorylation in renal collecting duct cells. *Journal of cell science* **113 (Pt 11)**, 1985-1992 (2000).

90. Zelenina, M. *et al.* Prostaglandin E(2) interaction with AVP: effects on AQP2 phosphorylation and distribution. *American journal of physiology. Renal physiology* **278**, F388-394 (2000).

91. Kamsteeg, E. J. *et al.* Short-chain ubiquitination mediates the regulated endocytosis of the aquaporin-2 water channel. *Proceedings of the National Academy of Sciences of the United States of America* **103**, 18344-18349, doi:10.1073/pnas.0604073103 (2006).

92. Pearl, M. & Taylor, A. Actin filaments and vasopressin-stimulated water flow in toad urinary bladder. *The American journal of physiology* **245**, C28-39 (1983).

93. Ding, G. H., Franki, N., Condeelis, J. & Hays, R. M. Vasopressin depolymerizes F-actin in toad bladder epithelial cells. *The American journal of physiology* **260**, C9-16 (1991).

94. Holmgren, K., Magnusson, K. E., Franki, N. & Hays, R. M. ADH-induced depolymerization of F-actin in the toad bladder granular cell: a confocal microscope study. *The American journal of physiology* **262**, C672-677 (1992).

95. Simon, H., Gao, Y., Franki, N. & Hays, R. M. Vasopressin depolymerizes apical F-actin in rat inner medullary collecting duct. *The American journal of physiology* **265**, C757-762 (1993).

96. Yui, N., Lu, H. J., Bouley, R. & Brown, D. AQP2 is necessary for vasopressin- and forskolin-mediated filamentous actin depolymerization in renal epithelial cells. *Biology open* **1**, 101-108, doi:10.1242/bio.2011042 (2012).

97. Klussmann, E. *et al.* An inhibitory role of Rho in the vasopressin-mediated translocation of aquaporin-2 into cell membranes of renal principal cells. *The Journal of biological chemistry* **276**, 20451-20457, doi:10.1074/jbc.M010270200 (2001).

98. Tamma, G. *et al.* Rho inhibits cAMP-induced translocation of aquaporin-2 into the apical membrane of renal cells. *American journal of physiology. Renal physiology* **281**, F1092-1101 (2001).

99. Tamma, G. *et al.* cAMP-induced AQP2 translocation is associated with RhoA inhibition through RhoA phosphorylation and interaction with RhoGDI. *Journal of cell science* **116**, 1519-1525 (2003).

100. Forget, M. A., Desrosiers, R. R., Gingras, D. & Beliveau, R. Phosphorylation states of Cdc42 and RhoA regulate their interactions with Rho GDP dissociation inhibitor and their extraction from biological membranes. *The Biochemical journal* **361**, 243-254 (2002).

101. Dong, J. M., Leung, T., Manser, E. & Lim, L. cAMP-induced morphological changes are counteracted by the activated RhoA small GTPase and the Rho kinase ROKalpha. *The Journal of biological chemistry* **273**, 22554-22562 (1998).

102. Szaszak, M., Christian, F., Rosenthal, W. & Klussmann, E. Compartmentalized cAMP signalling in regulated exocytic processes in non-neuronal cells. *Cellular signalling* **20**, 590-601, doi:10.1016/j.cellsig.2007.10.020 (2008).

103. Klussmann, E., Maric, K., Wiesner, B., Beyermann, M. & Rosenthal, W. Protein kinase A anchoring proteins are required for vasopressin-mediated translocation of aquaporin-2 into cell membranes of renal principal cells. *The Journal of biological chemistry* **274**, 4934-4938 (1999).

104. Uawithya, P., Pisitkun, T., Ruttenberg, B. E. & Knepper, M. A. Transcriptional profiling of native inner medullary collecting duct cells from rat kidney. *Physiological genomics* **32**, 229-253, doi:10.1152/physiolgenomics.00201.2007 (2008).

105. Klussmann, E. & Rosenthal, W. Role and identification of protein kinase A anchoring proteins in vasopressin-mediated aquaporin-2 translocation. *Kidney international* **60**, 446-449, doi:10.1046/j.1523-1755.2001.060002446.x (2001).

106. Henn, V. *et al.* Identification of a novel A-kinase anchoring protein 18 isoform and evidence for its role in the vasopressin-induced aquaporin-2 shuttle in renal principal cells. *The Journal of biological chemistry* **279**, 26654-26665, doi:10.1074/jbc.M312835200 (2004).

107. Rieg, T. *et al.* Adenylate cyclase 6 determines cAMP formation and aquaporin-2 phosphorylation and trafficking in inner medulla. *Journal of the American Society of Nephrology : JASN* **21**, 2059-2068, doi:10.1681/ASN.2010040409 (2010).

108. Giles, R. H., Ajzenberg, H. & Jackson, P. K. 3D spheroid model of mIMCD3 cells for studying ciliopathies and renal epithelial disorders. *Nature protocols* **9**, 2725-2731, doi:10.1038/nprot.2014.181 (2014).

109. Smith, F. D., Samelson, B. K. & Scott, J. D. Discovery of cellular substrates for protein kinase A using a peptide array screening protocol. *The Biochemical journal* **438**, 103-110, doi:10.1042/BJ20110720 (2011).

110. Ran, F. A. *et al.* Genome engineering using the CRISPR-Cas9 system. *Nat Protoc* **8**, 2281-2308, doi:10.1038/nprot.2013.143 (2013).

111. Doench, J. G. *et al.* Rational design of highly active sgRNAs for CRISPR-Cas9-mediated gene inactivation. *Nat Biotechnol* **32**, 1262-1267, doi:10.1038/nbt.3026 (2014).

Vita

Jennifer Whiting was raised in Northwood, NH and graduated from Coe-Brown Northwood Academy in 2005. She attended Rensselaer Polytechnic Institute in Troy, NY, where she graduated in 2009 with a BS in Biology. She conducted independent undergraduate research on *C. elegans* motor neuron development under the mentorship of Dr. Fern Finger. She was a summer student at the Jackson Laboratory in Bar Harbor, ME during the summer of 2008, where she used bioinformatics and data mining techniques to study accelerated aging disorders with Terry Maddatu, DVM. After graduating from Rensselaer Polytechnic Institute in 2009, Jennifer moved to Seattle, WA. She entered the Department of Pharmacology doctoral program at the University of Washington in 2009 and earned a Doctor of Philosophy in 2015.